Small Molecule Modulators of Apoptosis

Small Molecule Modulators of Apoptosis

by

James Luccarelli

Submitted in Partial Fulfillment of the Requirements for the M.D. Degree with Honors in a Special Field

Spring, 2017

Area of Concentration: chemical biology, apoptosis, cancer

Project Advisor: Loren D. Walensky, MD PhD

Author's Prior Degrees: BS, MS, DPhil

I have reviewed this thesis. It represents work done by the author under my supervision and guidance.

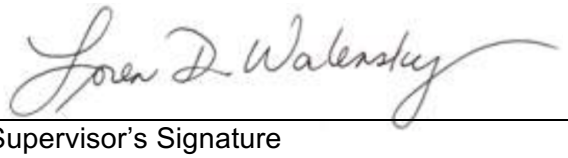

Faculty Supervisor's Signature

Authorship Statement

This thesis describes work conducted at the Dana-Farber Cancer Institute between February 2014 and February 2017, during which time I worked as a medical student and postdoctoral researcher in the Walensky Lab. Much of the described work was a collaborative effort with members of the lab. This thesis presents that portion of the work conducted by my own hands, or by graduate students or technicians working under my immediate supervision, except for the following:

Figure 2-3 panels B and D: data from F. Wachter, MD
Figure 2-4: peptides were designed and synthesised by E. Leshchiner, PhD
Figure 3-1: data from 2012 Walensky group screen
Figure 3-4 panels C-E: mass spectrometry performed by S. Lee, PhD
Figure 3-5: HXMS conducted by the Engen Lab of Northeastern University
Figure 4-3: Data from J. Pritz
Figure 4-4 panels A and B: data from J. Pritz

Portions of this work have already been published or submitted for publication:

Leshchiner, E.S.; Parkhitko, A.; Bird, G.H.; **Luccarelli**, **J**.; Bellairs, J.A.; Escudero, S.; Opoku-Nsiah, K.; Godes, M.; Perrimon, N.; Walensky, L.D. "Direct Inhibition of Oncogenic KRAS by Hydrocarbon-stapled SOS1 Helices." *Proc. Nat. Acad. Sci. U.S.A*. **2015**, *112*, 1761-1766.

Edwards, A.L; Wachter, F.; Lammert, M.; Huhn, A.J.; **Luccarelli, J**.; Bird, G.H.; Walensky, L.D. "Cellular Uptake and Ultrastructural Localization Underlie the Pro-Apoptotic Activity of a Hydrocarbon-stapled BIM BH3 Peptide." *ACS Chem. Biol.* **2015**, *10*, 2149-2157.

Lee, S.; Wales, T.E.; Escudero, S.; Cohen, D.T.; **Luccarelli, J**.; Gallagher, C.G.; Cohen, N.A.; Huhn, A.J.; Bird, G.H.; Engen, J.R.; Walensky, L.D. "Allosteric Inhibition of Antiapoptotic MCL-1." *Nat. Struct. Mol. Biol.* **2016**, *23*, 600-607.

Pritz, J.R.; Wachter, F.; Lee, S.; **Luccarelli, J.**; Cohen, D.T.; Wales, T.E.; Engen, J.R.; Heffron, G.J.; Massefski, W.; Walensky, L.D. "Allosteric Sensitization of Pro-Apoptotic Bax." *Nat. Chem. Biol. Accepted.*

Escudero, S.; Lee, S.; Mill, C.P.; Morgan, A.M.; Crawford, E.B.; **Luccarelli, J.;** Mourtada, R.; Oo, T.; Bird, G.H.; Zhang, Y.; Szarama, K.B.; Schuetz, J.D.; Opferman, J.T.; Walensky, L.D. *Submitted.*

James Luccarelli

Table of Contents

Small Molecule Modulators of Apoptosis

Abstract

Control of cell survival relies on a delicate balance between pro-apoptotic and anti-apoptotic signalling. In humans, the key regulatory proteins are those of the BCL-2 family, which include effector proteins such as BAX and BAK, anti-apoptotic proteins including BCL-2 and MCL-1, and pro-apoptotic proteins including BID and BIM. Dysregulation of apoptosis is among the Hallmarks of Cancer, and modulation of apoptosis holds promise as an effective therapeutic strategy for a range of malignancies. This thesis advances new strategies for modulating apoptosis using small molecules.

The first section explores the properties of stapled peptides. These molecules incorporate two non-natural amino acids with olefin sidechains that are then covalently linked. The resulting "staple" modifies the biophysical properties of the molecule. This chapter shows how stapling results in greater serum stability of the peptides, improves binding affinity for anti-apoptotic targets, and allows for facile transformation of a native sequence into an improved peptide, as demonstrated by stapling a SOS1 peptide to target KRAS.

The second section targets MCL-1, an antiapoptotic BCL-2 family protein that has emerged as a major pathogenic factor in human cancer. MCL-1 bears a surface groove whose function is to sequester the BH3 killer domains of proapoptotic BCL-2 family members, but successful drugging of this groove has not been achieved. This chapter develops an alternative strategy using a small molecule that covalently modifies C286 at a novel interaction site distant from the BH3-binding groove. This allosteric mechanism results in reduced BH3 binding capacity of MCL-1 and impairs the oncogenic anti-apoptotic activity of the protein.

The final chapter targets BAX, a critical executioner protein in the apoptotic pathway whose oligomerization causes permeabilization of the mitochondrial outer membrane. Using STD-NMR, a library of nearly 1,000 fragments was screened for binding to full-length BAX. This resulted in the discovery of a compound BIF-44 that sensitizes BAX by engaging a noncanonical hydrophobic pocket formed by the junction of the α3-α4 and α5-α6 hairpins. Biochemical and structural analyses indicate that the molecule sensitizes BAX by allosterically mobilizing the α1-α2 loop, a mechanism implicated in the initiation of BH3-mediated direct BAX activation. The identified compound thus informs the mechanism for initiation of BAX activation, and provides a new opportunity to reduce the apoptotic threshold for potential therapeutic benefit.

Acknowledgements

I came to HMS an organic chemist with no knowledge of biology or medicine and no clear sense of where my career would take me. Four years later I'm amazed by how much I've learned and grown, and am more than a little shocked by my chosen specialty. So much of that is because of the colleagues I had the privilege of working with on this research, and to whom I owe so much.

First and foremost to Loren, who has shaped my medical school experience clinically, academically, professionally, and personally. I knew I wanted to work for you about 10 minutes into your HST pathology lecture, and I'm so fortunate you were willing to take on a student who questioned you about the magnitude of an HSQC shift on one of your slides. I regret that I won't be working directly with you on the wards in the years to come, but you are the model of the physician and scientist I hope to become.

I've had the great fortune of working with nearly every member of the Walensky lab on one project or another. Thanks for your enthusiasm for (some of) the harebrained ideas I've sketched out for you, and for your wisdom in not pursuing the not-so-smart ones. I know I was sometimes a whirlwind dropping into lab for brief moments and piling work on you, but your brilliance and passion for science was a huge motivator for me even when I was (mostly) physically elsewhere. Special shoutout to team BAX: I didn't exactly want to be swapping NMR tubes at 3am shortly before boards, but I'm glad I had you guys there with me when we did.

I am forever indebted to the HST program for teaching me to think like a biologist and a physician. In just 16 months in the classroom I learned far more than I thought possible. Particular thanks to Rick Mitchell and Bobby Padera, whose Pathology course is the best class

I've taken in the roughly 25 years I've spent in the classroom. Patty Cunningham in the HST office was my surrogate mother during medical school, and I appreciate her wisdom and guidance. Throughout, my HST and MD/PhD classmates were huge contributors, both intellectually and personally. I look forward to remaining your friend and colleague as we all continue our journeys to become physician-scientists.

Finally, to my family, who have continued to support me in yet another city that isn't New York. It'll be a few more years now that I've matched in Boston, and I appreciate your love.

Glossary of Abbreviations

Å – Angstrom

BAK – BCL-2 antagonist killer 1 (protein)

BAX – BCL-2-associated X (protein)

BCL-2 – B-cell lymphoma 2 (protein)

BCL-X_L – B-cell lymphoma-extra large (protein)

BH3 – BCL-2 homology domain 3

BIF – BAX-interacting fragment

C – Celsius

δ – chemical shift

D – deuterium

Da – Daltons

DCM – dichloromethane

DIPEA – ethyldiisopropylamine

DMSO – dimethylsulfoxide

FITC – fluorescein isothiocyanate

FP – fluorescence polarization

g – gram(s)

H – hydrogen

HPLC – high-performance liquid chromatography

HSQC – heteronuclear single quantum coherence

Hz – Hertz

HXMS – hydrogen/deuterium-exchange mass spectrometry

KRAS – Kirsten rat sarcoma viral oncogene homolog (protein)

LC – liquid chromatography

MAIM1 – MCL-1 allosteric inhibitory molecule 1

MCL-1 –myeloid cell leukemia sequence 1 (protein)

MD – molecular dynamics

MS – mass spectrometry

NMR – nuclear magnetic resonance

PDB – protein data bank

PEG – polyethylene glycol

PPI – protein-protein interaction

RMSD – root mean square deviation

RMSF – root mean square fluctuation

SAHB – stabilized alpha helix of BCL-2 domains

SOS – son of sevenless (protein)

STD – saturation transfer difference

TMS – tetramethyl silane

vMIA – viral mitochondria-localized inhibitor of apoptosis

1. Introduction

1.1. Programmed cell death

Ordinary homeostasis in multicellular organisms requires a delicate balance between cell proliferation and cell death. While some cells, including neurons and cardiomyocytes, live as long as the organism itself, others turnover in a matter of days (1). In humans, an estimated 5-7x10^{10} cells die daily, requiring exquisite control over death pathways (2). Indeed, inhibition of these essential pathways is one of the key "hallmarks" of cancer (3,4), making them of great clinical relevance.

One of the hallmarks of programmed cell death is the lack of the inflammatory response seen in tissue necrosis. Although this phenomenon had been described microscopically as early as the 1880s, the first scientific discussion came in 1972 (5), when the term apoptosis was coined. These early investigators noticed the characteristic changes by light microscopy that still define apoptotic death: cell shrinkage followed by chromatin condensation (pyknosis), nuclear fragmentation (karyorrhexis), and ultimately division into cell fragments or "apoptotic bodies." This is followed swiftly by phagocytosis by professional scavenger cells, which do not secrete inflammatory cytokines in response (6). In contrast, necrotic cell death proceeds to cell fragmentation (karyolysis) and activation of a potent immune response, which would be maladaptive in many of the circumstances where programmed cell death is required.

Molecular investigations into apoptosis were made possible by the model organism *C. elegans*, in which 131 of the overall 1090 cells are fated to die during development (7,8). Genetic investigation of these cells led to the discovery of a complicated series of genes that promote, prevent, or cause cell death. These include two death genes, *ced-3* and *ced-4*, which initiate cell death (9,10); a protective protein, *ced-9*, which prevents cell death (11); and a

regulator, *egl-1*, which suppresses the function of *ced-9* and promotes death (12). Homologues of each of these genes have been found in higher organisms, where they are joined by many other related genes, yielding a detailed understanding of a complicated web of apoptotic interactions in humans.

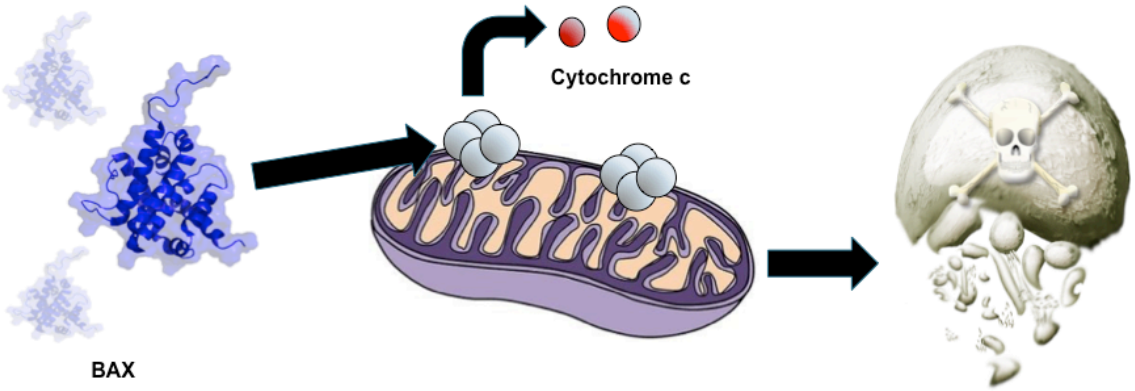

Figure 1-1: Mechanism of apoptotic signaling. Ordinarily BAX is cytosolic, but once activated it forms a pore of unknown structure in the outer mitochondrial membrane, causing the release of cytochrome C. This causes activation of downstream caspases, ultimately leading to apoptotic cell death.

The key organizing point for apoptosis is the mitochondrion. Under normal circumstances the mitochondrion sequesters cytochrome C (part of the electron transport chain), an essential cofactor for the death-inducing caspases (homologues of *ced-3* and *ced-4*) (13). During apoptosis, the mitochondrial membrane becomes permeabilized to cytochrome C release, thereby activating the downstream destruction of DNA. As a result, numerous regulatory mechanisms function at the level of the mitochondrial membrane. Cytochrome C release occurs via the formation of a membrane "effector" pore of unknown structure. These pores are formed by the activated pro-apoptotic proteins BCL-2 antagonist killer 1 (BAK) or BCL-2-associated X protein (BAX), which oligomerize on the mitochondrial outer membrane (Figure 1-1). The action of these effector proteins is kept in check by numerous antiapoptitic proteins, which are homologues of the products of the *ced-9* gene. The prototypical example of

these is B-cell lymphoma 2 (BCL-2) first discovered at the t(14;18) breakpoint in follicular lymphoma (14,15).

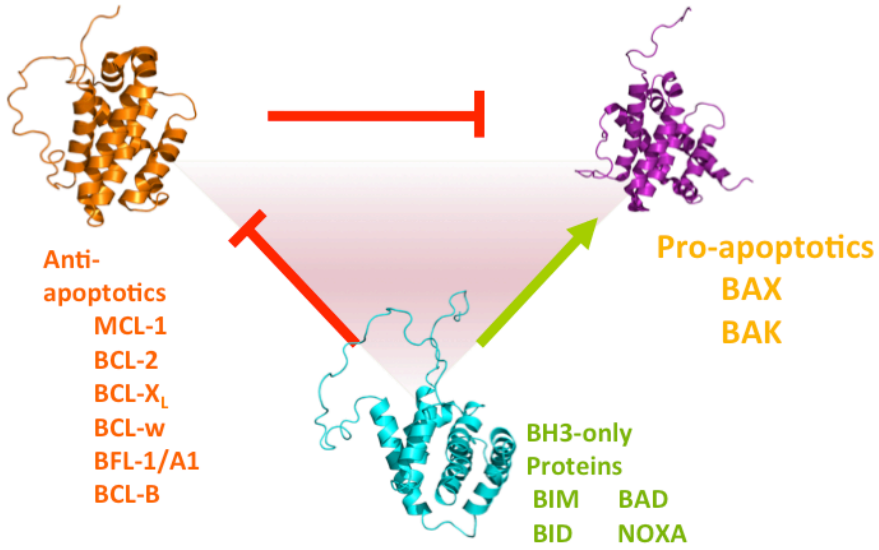

Figure 1-2: BCL-2 family proteins involved in apoptosis. The anti-apoptotic proteins suppress the activity of pro-apoptotic BAX and BAK and sequester the BH3-only proteins. BH3-only proteins bind to both pro-apoptotic and anti-apoptotic family members. Determination of cell fate relies in part on the quantity and localization of each of the family members.

The interplay between pro-apoptotic and anti-apoptotic proteins is mediated by activator BH3-only proteins (homologues of *egl-1;* Figure 1-2). These BH3-only proteins are intrinsically disordered, but become structured upon binding to their targets (16). When bound to effector proteins, BH3-only proteins promote oligomerization and pore formation, and thus cell death (17). In contrast, the BH3-only proteins can also bind and be sequestered by BCL-2 family anti-apoptotic proteins, thereby preventing activation of BAX and BAK (18). Other BH3-only proteins, termed sensitizers, cannot directly activate pore formation, but only bind to and sequester BCL-2 family proteins (19). Whether a particular BH3-only signal will be sequestered or lead to apoptosis depends on the cellular locations, concentrations, and affinities of all of the possible binding partners. Quantitative "BH3-profiling" attempts to track the particular balance of these signals in any particular cell, thereby predicting response to therapeutics (20). Overexpression of select BCL-2 family proteins confers resistance to

apoptosis, and is a causative mechanism in the development and chemoresistance of many human neoplasms (21).

The anti-apoptotic BCL-2 family members include the related BCL-2, BCL-x_L, BCL-w, BFL-1, and MCL-1 proteins (Figure 1-2). Certain tumors are dependent on the action of a single of these proteins (for instance, CLL requires BCL-2), allowing for a selective inhibitor to have clinical efficacy (22). In contrast, many other cancers can survive using several BCL-2 proteins, requiring deactivation of multiple in order to reactivate apoptosis. As most cancer therapeutics function by inducing the intrinsic apoptotic pathway in susceptible tumor cells, activation of these pathways is an important goal (23). The first effective drug targeting BCL-2, venetoclax, was FDA-approved in 2016 (24). Potent pan-inhibitors of BCL-2, BCL-X_L, and BCL-w have also been developed, but MCL-1 activation rapidly promotes resistance (25). Moreover, somatic mutations of MCL-1 have been found across a range of human cancers (26), making it a promising target for cancer therapeutics.

1.1.1. MCL-1

MCL-1 (myeloid cell leukemia sequence 1) was first discovered as a protein supporting viability during myeloid cell differentiation (27). It shares structural similarity to BCL-2 but different tissue expression patterns (28). Relative to other BCL-2 family proteins, MCL-1 has a relatively short half life and is extensively regulated by expression levels and post-translational modifications (29). MCL-1 is generally localized to the mitochondrial outer membrane, where it binds and sequesters BAK and prevents pore formation (30). The addition of a BH3-only ligand can displace BAK from MCL-1, thereby activating cell death pathways. In malignancies MCL-1 may be overexpressed, promoting cell survival despite pro-apoptotic signaling. This can leave a cell "primed for death" as huge quantities of BH3-only peptides are present, though

sequestered. In this state, removal or deactivation of even relatively small amounts of the anti-apoptotic proteins can lead to rapid cell death as the abundant BH3-only domains are released (31).

A great deal is known about the structure of MCL-1, with more than 30 crystal or NMR structures of the protein deposited in the PDB. These include apo structures, as well as complexes of MCL-1 with a variety of peptide and small molecule binders. Although MCL-1 shares only ~25% sequence homology with BCL-2, structurally the two have very similar folds (32). This includes a central α helix surrounded by six additional helices. Portions of four of these helices contribute to the binding pocket for BH3 peptides, and form extensive hydrophobic contact with the peptides. The addition of a BH3 ligand stretches open the binding pocket by ~0.5 nm relative to the unbound state (33). Additionally there is an unstructured transmembrane domain that helps localize MCL-1 to the outer mitochondrial membrane, and which is usually truncated for structural studies.

1.1.2. BAX

BAX is a 21 kDa globular protein composed of nine α-helices that functions as a critical effector of the BCL-2 family-regulated mitochondrial apoptotic pathway. It was discovered in 1993 as a heterodimer with BCL-2 (34), and was found to activate apoptosis. Later work established that BAX binds to other anti-apoptotic proteins, leading to the theory that the ratio of these proteins determined cell death (35). BAX is generally localized in the cytosol, but on activation translocates to the mitochondrial outer membrane (36). Once there it can be retrotranslocated by BCL-X_L back to the cytosol (37).

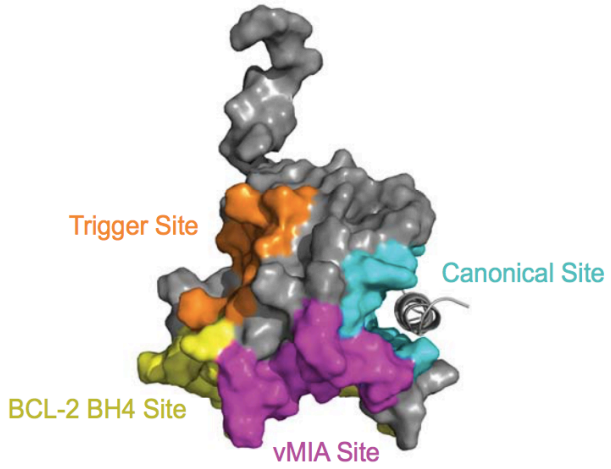

Figure 1-3: The structure of BAX. BAX contains a series of surface grooves that regulate its pro-apoptotic activity, including BH3-binding trigger (orange) and canonical (cyan) sites, and inhibitory BCL-2 BH4 (yellow) and vMIA (purple) interaction pockets. Figure adapted from Pritz *et al*. (accepted).

For such a small protein, a surprisingly large series of regulatory surfaces and complex conformational changes have been defined (Figure 1-3). Indeed, the inherent risk to the cell of renegade BAX activation may underlie the mechanistic basis for its multifaceted regulation. Structurally BAX has a hydrophobic core formed by an α5/α6 hairpin (38). In the resting cytosolic state, the canonical BH3 binding groove composed of portions of α-helices 2, 3 and 4 of BAX is occupied by the protein's own α9 helix (Figure 1-3, cyan), which is exposed upon activation and inserts into the membrane. Cytosolic activation is mediated by a "trigger site" on the opposite face of the protein (39), between α-helices 1 and 6 (Figure 1-3, orange). In response to stress, BH3-only direct activator proteins, such as BIM, BID, and PUMA, can directly and sequentially engage the α1/α6 trigger site and canonical hydrophobic groove to initiate and propagate BAX homo-oligomerization (40).

In addition to the activation domains, BAX is negatively regulated by vMIA, a cytomegalovirus protein implicated in blocking BAX-mediated apoptosis. This ensures host cell survival during viral infection and replication (41). The BAX-binding domain of vMIA achieves its inhibitory effect by binding to a discrete pocket formed by the flexible loops

between helices α1/α2, α3/α4, and α5/α6 and a portion of the C-terminal α9 helix (Figure 1-3, purple), preventing BAX-activating conformational changes by stabilizing the α3/α4 and α5/α6 hairpins (42). Additionally, the BH4 motif of BCL-2 can also bind and inhibit BAX at a separate interface (Figure 1-3; yellow) defined by helix α1, the α1/α2 loop, and α2/α3 and α5/α6 hairpins (43).

1.2. Strategies towards inhibitors of protein-protein interactions

It is clear that the development of chemical modulators of apoptosis may be an important advance in cancer and other diseases. Unfortunately, the nature of the relevant protein-protein interactions (PPIs) makes therapeutic discovery challenging. Most traditional medicinal chemistry efforts have focused on enzymes, which by virtue of having a defined active site are often targetable with small molecules. In contrast, protein-protein interactions present a much more challenging target: the interacting surfaces are large, generally lack defined binding pockets, and form extensive non-covalent contacts (44,45). Despite these challenges, the discovery of "hot spots"—individual residues which contribute the majority of binding energy along a PPI surface—has made the search for inhibitors of PPIs possible (46). By carefully targeting these key regions of the interaction surface, even large PPIs have been successfully inhibited (47,48).

Diverse approaches including high throughput screening (49), fragment screens (50), computational simulations (51), and covalently modified peptides (52) have all been applied to seek MCL-1-selective inhibitors, but unfortunately the efficacy of many these molecules remains low (53). Other potential approaches draw inspiration from the known peptide binders. The majority of the free energy of binding of helical proteins comes from sidechain, rather than backbone, interactions (54,55), so synthetic molecules which display sidechains with the same

spatial and angular orientation as a BH3 ligands may prove useful. Several such peptidomimetics have been found to bind to the related Bcl-X_L, including terphenyl (56,57), oligopyridylamide (58), terephthalamide (59), benzoylurea (60), biphenyl (61), and "wet edge" (62) scaffolds (Figure 1-4).

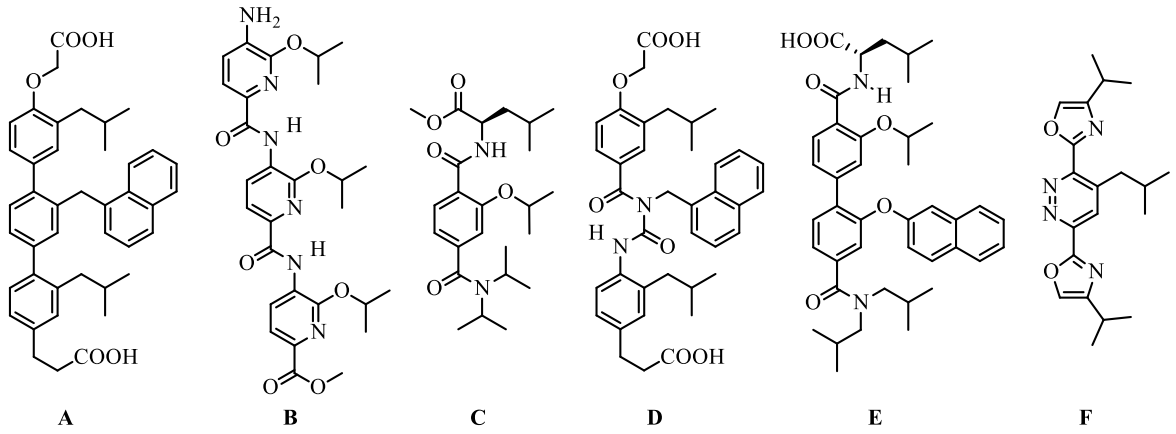

Figure 1-4: Different peptidomimetics which bind to Bcl-X_L. (a) terphenyl, K_i 0.114 μM. (b) oligopyridylamide, K_i 2.3 μM. (c) terephthalamide, K_i 0.781 μM. (d) benzoylurea, K_i 2.4 μM. (e) biphenyl, K_i 1.8 μM. (f) "wet-edge" mimic, K_i not determined.

1.2.1. Stapled peptides

An alternative approach involves covalently modifying peptide sequences with an olefin linker (Figure 1-5). These "stapled peptides" display increased helicity and resistance to proteolytic degradation compared to native sequences (63,64). An initial study identified a stapled peptide binder of MCL-1 in 2010 (65). This study screened stapled peptides based on pro-apoptotic BH3 domains, and found that the BH3 domain of MCL-1 itself was the most potent binder to the BH3 pocket of MCL-1. The peptide with the highest affinity was successfully co-crystallized with MCL-1 and its structure solved by X-ray crystallography. Using this structure, detailed molecular calculations using free energy perturbation methods have attempted to improve on the affinity of these helices (51), but experimental verification is lacking.

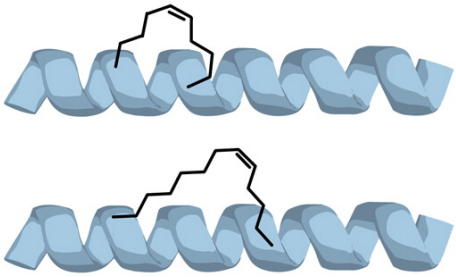

Figure 1-5: Chemical "stapling" of a helix using a hydrocarbon linker. The resulting stapled peptide is constrained to a more helical conformation, with resulting changes in the pharmacokinetic and pharmacodynamic properties of the molecule. Figure adapted from an open access figure by Bird and Walensky (66).

Significant questions remain regarding the suitability of stapled peptides as potential therapeutics. In particular, while stapling can clearly improve the binding affinity of a peptide, the staple position is a critical variable (63). Dozens of studies have now accumulated a great deal of evidence as to the suitability of different sequences for stapling (66), but controversy still remains regarding particular sequences. A recent debate in the literature has focused on the binding of the BH3 peptide of BIM to MCL-1, and has questioned the cell permeability and affinity of the modified molecules (67–70). More detailed investigations into this well-characterized system may help elucidate general principles regarding stapled peptides.

1.2.2. Covalent modifiers

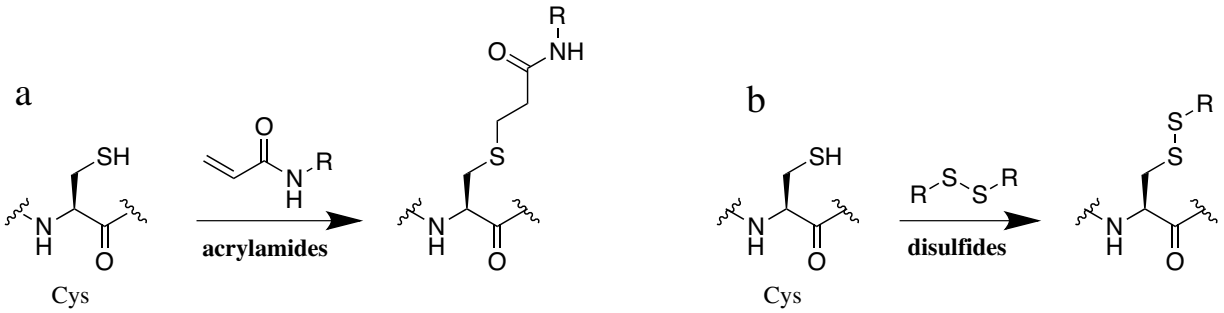

Figure 1-6: Covalent modification of cysteine. Reaction with activated α,β-unsaturated carbonyl compounds such as acrylamides (a), or disulfide exchange with disulfides (b) leads to covalent modification of the amino acid cysteine.

Additionally, a growing drive in medicinal chemistry is towards covalent modifiers of proteins. A covalent compound is by definition a non-competitive inhibitor, since once bound it has no appreciable dissociation rate and thus cannot be overcome even with high concentrations of native substrate. Moreover, covalent inhibitors may be more difficult to evolve resistance against (71), although concerns with off-target effects have limited the popularity of such molecules among medicinal chemistry programs. In general, reactive sidechains on proteins are most amenable to covalent modification, none more so than cysteine (Figure 1-6). Its nucleophilic sulfhydryl group makes it unique among natural amino acids in its reactivity towards electrophiles (72), which combined with its relative low natural abundance makes it an attractive target for covalent modifiers (73).

1.3. Thesis goals

The development and clinical adoption of the selective small molecule inhibitor of BCL-2, venetoclax, has proven the potential clinical utility of apoptosis modulators in cancer. Despite its success, most of the complicated web of cell death protein-protein interactions cannot presently be targeted by small molecule probes or therapeutics. This thesis seeks to extend the range of tool compounds available to chemical biologists. It begins with an exploration of the biophysical properties of stapled peptides and their applications to proteins of interest in cancer. It then moves to the discovery of an allosteric site on MCL-1 that is successfully targeted with a small covalent molecule. The work concludes with efforts to modify the activity of BAX using fragment-based screening to identify new classes of modulators of this apoptotic effector. In all sections, the properties of the molecules are investigated using a combination of biochemical, biophysical, and computational techniques.

2. Biophysical properties of stapled peptides

2.1. Introduction

Peptides adopt a variety of conformation in solution depending on the primary sequence of the chain. Some sequences have particular propensities to form particular conformations, for instance, the extended polyproline type II helix formed by repeated sequences of the amino acid proline (74). Among PPIs, the α-helix is likely the most common interaction motif, being present in approximately 40% of homodimeric interactions and 26% of heterodimeric interactions (75). This structure, first proposed by Pauling in 1951 (76) (although with the incorrect absolute configuration of amino acids (77)) and experimentally-verified in the crystal structure of myoglobin in 1960 (78), features 3.6 amino acids per turn, rising 5.4 Å between adjacent turns (Figure 2-1). In order to improve the helicity of this sequence, Verdine and colleagues applied a hydrocarbon "staple" to tether the helical structure to itself (79). These modified peptides were first applied to the BH3 domains critical to apoptosis (63), and since then have been applied to numerous other targets and sequences (66).

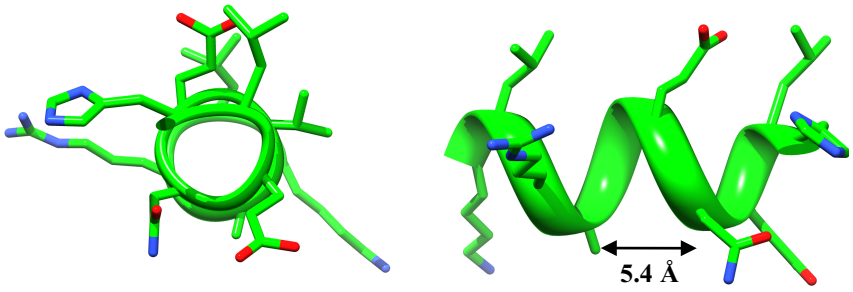

Figure 2-1: Structure of the α-helix, consisting of approximately 5.4 Å per turn, with each turn consisting of 3.6 amino acids. This results in an asymmetrical helix with sidechains projected radially around the axis of the peptide.

Dozens of studies of stapled peptides over the last 15 years have explored the effects of stapling on the properties of a peptide. The key conclusion of these studies is that stapling is not a panacea, but rather can have positive or negative effects on the desired or undesired

properties of any given sequence (66). To further demonstrate these effects, a head-to-head study was conducted on the biophysical and biochemical properties of two stapled peptides (termed "stabilized α-helices of BCL-2 domains," or SAHBs; Figure 2-3A) modeled after the BH3 domain of the pro-apoptotic protein BIM (70). The first of these, BIM $SAHB_{A1}$, encompasses amino acid residues 146–166 of the BH3 domain and was found to have notably high α-helicity in aqueous solution and low nanomolar binding affinity for its BCL-2 family protein targets (80). This peptide had such high affinity for its targets that it could not be used for NMR binding studies due to overly-tight binding, so a second sequence (BIM $SAHB_{A2}$ aa 145–164) was generated with relatively lower α-helical content in solution and a negative charge (39). Using these related, but distinct, sequences along with their unstapled control peptides allows for direct comparison of the possible effects of stapling. Additionally, NMR structural studies were undertaken using a novel stapled SOS1 peptide targeted towards the oncogenic protein KRAS (81).

2.2. Methods

2.2.1. Protease stability

In vitro proteolytic degradation was measured by LC/MS (Agilent 1200) using the following parameters: 20 µl injection, 0.6 ml flow rate, 15-minute run time consisting of a gradient of water (0.1% formic acid) to 20%–80% acetonitrile (0.75% formic acid) over 10 minutes, 4-minute wash to revert to starting gradient conditions, and 0.5-minute post-time. Reaction samples were composed of 5 µl peptide in DMSO (1 mM stock) and 195 µl buffer consisting of 50 mM $(NH_4)_2CO_3$, pH 7.4. Upon injection of the 0-hour time sample, 2 µl of 50 ng/µl ASP-N protease (Sigma-Aldrich) was added, and the amount of intact peptide was quantitated by serial injection over time. A plot of peak area versus time yielded an exponential

decay curve, and half-lives were determined by nonlinear regression analysis using Prism software (GraphPad).

2.2.2. Stapled peptide synthesis and characterization by CD

All-hydrocarbon stapled peptides were synthesized; derivatized at the N-terminus with FITC, Ac, or Biotin-PEG; and purified to >95% homogeneity by LC/MS as previously described (68). Acetylated peptides were dissolved in 20% (v/v) acetonitrile in water for circular dichroism analyses, performed on an Aviv Biomedical spectrophotometer.

2.2.3. BCL-X_L protein production

BCL-X_L ΔC was expressed as a glutathione-S-transferase (GST) fusion protein in *Escherichia coli* BL21 (DE3) from the pGEX2T vector (Pharmacia Biotech) and purified by affinity chromatography using glutathione sepharose beads (GE Healthcare), followed by thrombin cleavage of the GST tag. Pure, monomeric protein was isolated by gel filtration FPLC.

2.2.4. Fluorescence polarization binding assay

For direct FP binding assays, FlTC-derivatized BIM BH3 peptides (50 nM) were added to serial dilutions of recombinant protein in binding buffer (BCL-X_L ΔC: 100 mM NaCl, 50 mM Tris, pH 8.0; full-length BAX and BCL-X_L: 140 mM NaCl, 50 mM Tris, pH 7.4) in 96-well black opaque plates. The plates were incubated in the dark at RT and then fluorescence polarization measured at 20 min on a microplate reader (SpectraMax M5 Microplate Reader, Molecular Devices). Dissociation constants (K_D) were calculated by nonlinear regression analysis of dose–response curves with Prism software 5.0 (GraphPad) using the ligand depletion formula for FP binding assays, as described (82).

2.2.5. KRAS protein production

Recombinant wild-type human KRAS protein (amino acids1–156) was expressed in *Escherichia coli* BL21(DE3) as an N-terminal hexahistidine-tagged (His_6) fusion protein by using the pET28-MHL expression vector (Addgene plasmid 25153; a gift from C. Arrowsmith, University of Toronto, Toronto). Protein expression was induced with 1 mM IPTG for 4 h at 30 °C. Bacterial pellets were resuspended in lysis buffer (20 mM Tris, 250 mM NaCl, pH 7.6), lysed by microfluidization (Microfluidics M-110L), and centrifuged at 45,000 rpm for 1 h at 4 °C (Beckman L-90K). The cleared cellular lysates were subjected to Ni affinity resin (Qiagen) chromatography followed by elution with 150 mM imidazole in 50 mM Tris, 250 mM NaCl, pH 7.8. Concentrated eluates were subjected to size exclusion chromatography (GE Life Sciences) at 4 °C by using 50 mM Tris, 150 mM NaCl, pH 7.8 buffer conditions, and the corresponding monomeric peaks were collected. Protein concentration was determined by Bradford assay (Bio-Rad) and UV absorbance measurements, and the average value was used. His_6-tagged KRAS proteins were used in all biochemical experiments unless otherwise indicated. Purified KRAS protein (200 μM) was incubated with 2 mM GDP or GppNp in loading buffer [20 mM Tris · HCl (pH 7.5), 150 mM NaCl, 5 mM EDTA, 1 mM DTT] for 1.5 h on ice. Reactions were quenched with 12 mM $MgCl_2$ and incubated for 30 min on ice.

2.2.6. NMR spectroscopy:

All spectra were collected by using an Agilent Inova 500 MHz system equipped with a triple resonance (H, C, N) 5-mm cold probe. Experiments were performed at 25 °C. KRAS was uniformly ^{15}N isotopically labeled, charged with GDP as described above, and dissolved in phosphate buffer (95:5 H_2O:D_2O, PBS pH 7.4, 1.0 mM DTT, 2 mM $MgCl_2$). The instrument was locked to the deuterium signal, and resonances are reported in parts per million relative to

D_2O (δ_H = 4.72 ppm). A 5-mm NMR tube was charged with 500 μL of sample (100 μM protein) and the ^{15}N-heteronuclear single quantum correlation (HSQC) spectrum was recorded. Resonances were compared with the literature values (83). For titration experiments, up to 10 molar equivalents of SAH-SOS1$_A$ (in PBS) were added to the protein solution. Data were analyzed by using VNMRJ 3.2 software (Agilent Technologies). The change in chemical shift upon addition of ligand was plotted for each KRAS residue. The chemical shifts of ^1H and ^{15}N were averaged by using the formula:

$$Shift = \sqrt{0.5 \times [\delta_H^2 + (\alpha \times \delta_N^2)]}$$

with the scale factor α taken to be 0.14 (84). The absence of a bar indicates no chemical shift change, the presence of a proline, or a residue that is overlapped or not assigned.

2.2.7. Docking calculations

The peptide sequence FFGIXLTNXLKTEEGN was built by using Maestro in an idealized α-helical form. The sequence was docked to the target protein by using the HADDOCK webserver default parameters (85,86). Chain R of the 1NVU crystal structure was used (87), with residues L6, G15, H27, F28, V29, L56, D57, E63, Y64, R73, T74, G77, and R149 defined as the active residues. Top-scoring clusters were analyzed visually with Pymol (Schrödinger, LLC).

2.3. Results and discussion

2.3.1. Stapling improves BIM peptide stability towards proteolysis

To test the serum stability of the stapled peptides versus the native sequences, the peptides were dissolved in buffer and added to ASP-N protease, which selectively cleaves at the N terminus of Asp and Cys residues. Only a single Asp is present in the BIM sequences,

and is located between the two residues which constitute the staple. As an additional control, the BIM sequence incorporating the non-natural quaternary aliphatic amino acids that constitute the staple, but not undergoing the ring-closing stapling reaction, was included.

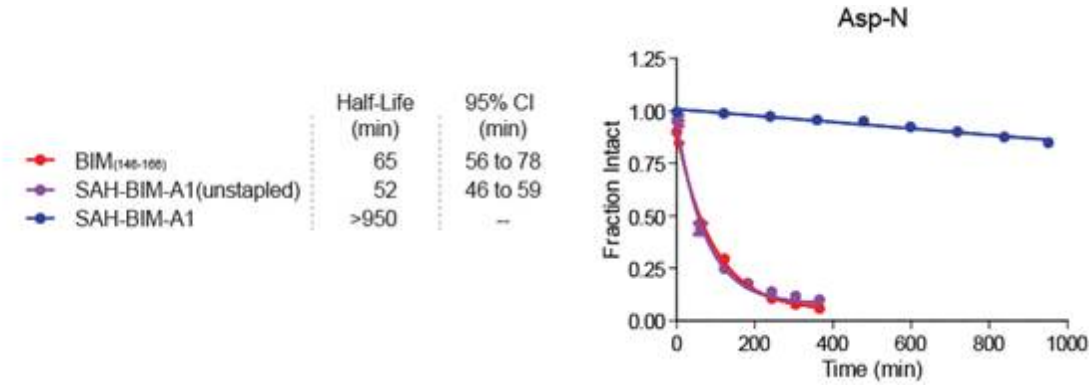

Figure 2-2: Stability of the native BIM peptide, BIM peptide substituted with non-natural quaternary aliphatic amino acid, and the substituted and stapled peptide to degradation with the ASP-N protease. The native and substituted peptides showed equal propensity to cleavage by the protease, but the stapled peptide remained >80% intact after 16 hours. Figure adapted from Edwards *et al*. (70).

Results (Figure 2-2) indicate that only the stapled peptide, but not the unmodified or modified but unstapled sequences, displays resistance to proteolysis. Stapling increases the serum half life by more than a factor of 15, with less than 25% degredation at 16 hours for the stapled peptide vs. near-complete degredation in 5 hours for the unstapled versions.

2.3.2. Stapled BIM peptides have increased helicity and improved binding affinity relative to unstapled peptides

The conformation of the BIM unmodified and stapled sequences were evaluated *via* circular dichroism. In this technique the characteristic conformations of a peptide are explored using the different absorbances of left-handed and right-handed circularly polarized light. In this case, the BIM stapled peptides both exhibit increased helicity relative to the unmodified forms (Figure 2-3B). As expected and designed, the A1 sequences display greater helicity than the A2 sequences.

The affinity of the sequences for the anti-apoptotic protein BCL-X_L was then measured. using a fluorescence polarization (FP) assay. This assay measures binding affinity based on the change in tumbling rate of a ligand when bound and unbound to a larger protein target (88). In the unbound form the ligand tumbles relatively fast in solution, meaning that when excited with polarized light it rotates and thus emits photons in a relatively unpolarized manner. When bound to a protein the tumbling rate is slower, so a higher fraction of the initial polarized photons remain in the polarized orientation. By varying protein concentration with a constant amount of ligand, a binding isotherm is generated from which a binding dissociation constant may be calculated. For this assay, both C-terminally truncated BCL-X_L and the full-length protein were used.

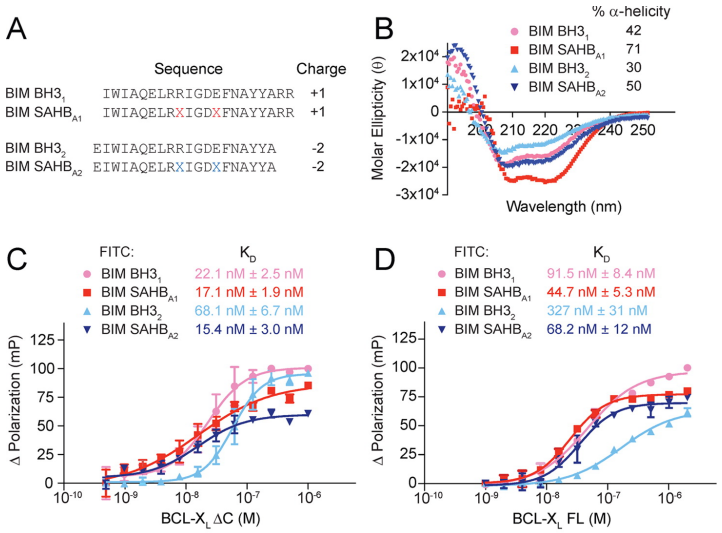

Figure 2-3: Comparative amino acid sequence, α-helical content, and BCL-2 family protein direct binding activities of BIM BH3 peptides. (A) Amino acid sequence and staple position of unmodified and stapled BIM BH3 peptides. (B) Circular dichroism analysis of unmodified and stapled Ac-BIM BH3 peptides, dissolved in 20% acetonitrile/water. (C–D) Comparative direct binding activities of FITC-BIM BH3 peptides for (C) BCL-X_L ΔC, (D) full-length (FL) BCL-X_L, as measured by FP assay. Plotted data are mean ± SD for experiments performed in triplicate; K_D's are mean ± SEM of the calculated dissociation constants from biological replicates. Data panels B and D of this figure were obtained by F. Wachter, MD. Figure adapted from Edwards *et al*. (70).

Results (Figure 2-3C-D) indicated that as expected, the A1 sequences have higher affinities than the A2 helices. In each case, stapling results in an increase in binding affinity, although the effect size is modest in most instances. Binding affinities for the full-length

protein are uniformly worse than for the truncate, likely due to competition from the α9 helix for the binding pocket in the case of the full-length protein.

2.3.3. A SOS1 stapled peptide binds to KRAS at the SOS1 pocket

One strength of stapled peptide technology is its theoretical application to any helix found within a protein binding interface. Work within the Walensky lab has sought to use this approach towards non-apoptotic targets important in cancer. One such target is the RAS family of proteins, which play a critical role in a variety of cellular processes including cell survival, proliferation, and motility (89). In particular, the KRAS form is the most frequent oncogenic driver of the RAS forms and is associated with particularly poor prognosis in several cancer types including those of the pancreas, lung, and colon (90). RAS action is mediated by nucleotide exchange, and it is active in the GTP-bound form. Guanine-nucleotide exchange factors (GEFs) facilitate GDP release, and thus activate RAS by promoting GTP association. In particular, the GEF SOS1 is the rate-limiting step of KRAS function (91).

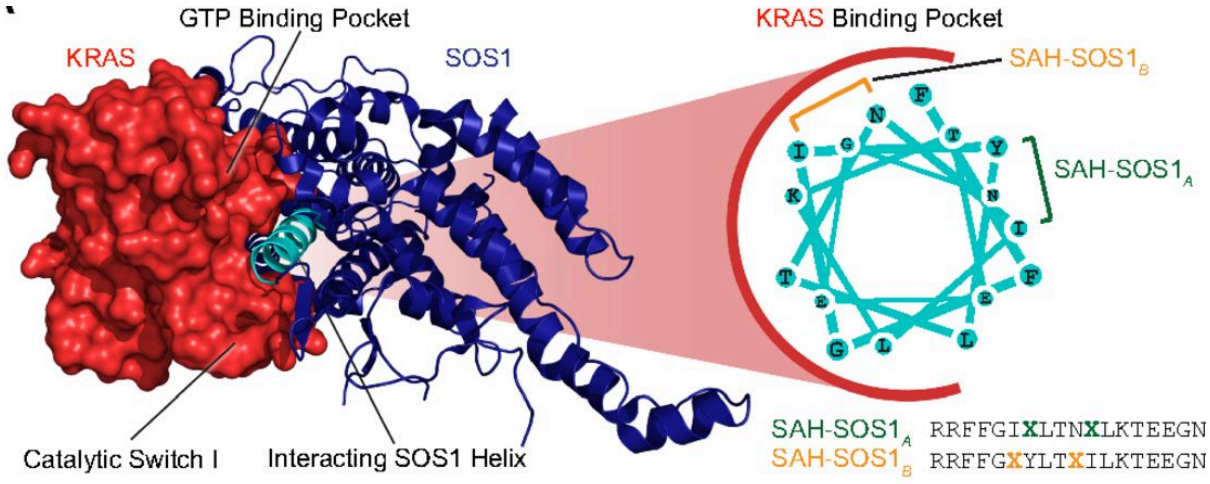

Figure 2-4: The crystal structure of KRAS (red) in complex with its guanidine exchange factor SOS1 (blue) reveals a binding interaction between the indicated SOS1 α-helix (cyan) and KRAS (PDB ID code 1NVU). SAH-SOS1 peptides were generated by inserting all-hydrocarbon staples at positions A (green) and B (orange) into a SOS1 peptide spanning amino acids 929–944 and bearing an N-terminal Arg-Arg tag to optimize cellular penetrance. These peptides were designed and synthesized by E. Leshchiner, PhD. Figure adapted from Leshchiner *et al*. (81).

A series of SOS1 stapled peptides were designed and synthesized by E. Leshchiner, PhD in the Walensky lab (Figure 2-4). These were found to bind to KRAS by FP, and this binding was shown to inhibit nucleotide exchange (81). A key remaining question was the binding site of these peptides. In order to explore this question, ^{15}N HSQC NMR experiments were conducted. In this technique, a protein is grown with ^{15}N isotopically-labeled residues. The NMR chemical shifts of the proton (^{1}H) and nitrogen (^{15}N) components of the backbone amides are then correlated. As NMR shifts are very sensitive to local chemical environment, changes in protein structure are readily detected (84). The binding of a ligand to the protein causes a change in the local chemical environment, resulting in a shift in one or both of the ^{1}H and ^{15}N resonances, thereby revealing the site of binding.

GDP-loaded ^{15}N-KRAS was incubated with the stapled SOS1 peptide (Figure 2-5). Relatively few residues shift, indicating an overall global retention of the protein fold. Upon ligand binding, the discrete chemical shifts occur in residues that are located within the native SOS1 binding site. To further explore the possible binding mode, a docking calculation was performed using the program HADDOCK (85,92). The calculated model structure derived from docking analyses demonstrated the juxtaposition of stapled peptide residues with the majority of residues that undergo chemical shift change, such as L6, G15, L56, D57, E63, Y64, R73, T74, and Q99. Taken together, these structural analyses implicate the SOS1-binding pocket of KRAS as the functional site of the SOS1 stapled peptide interaction.

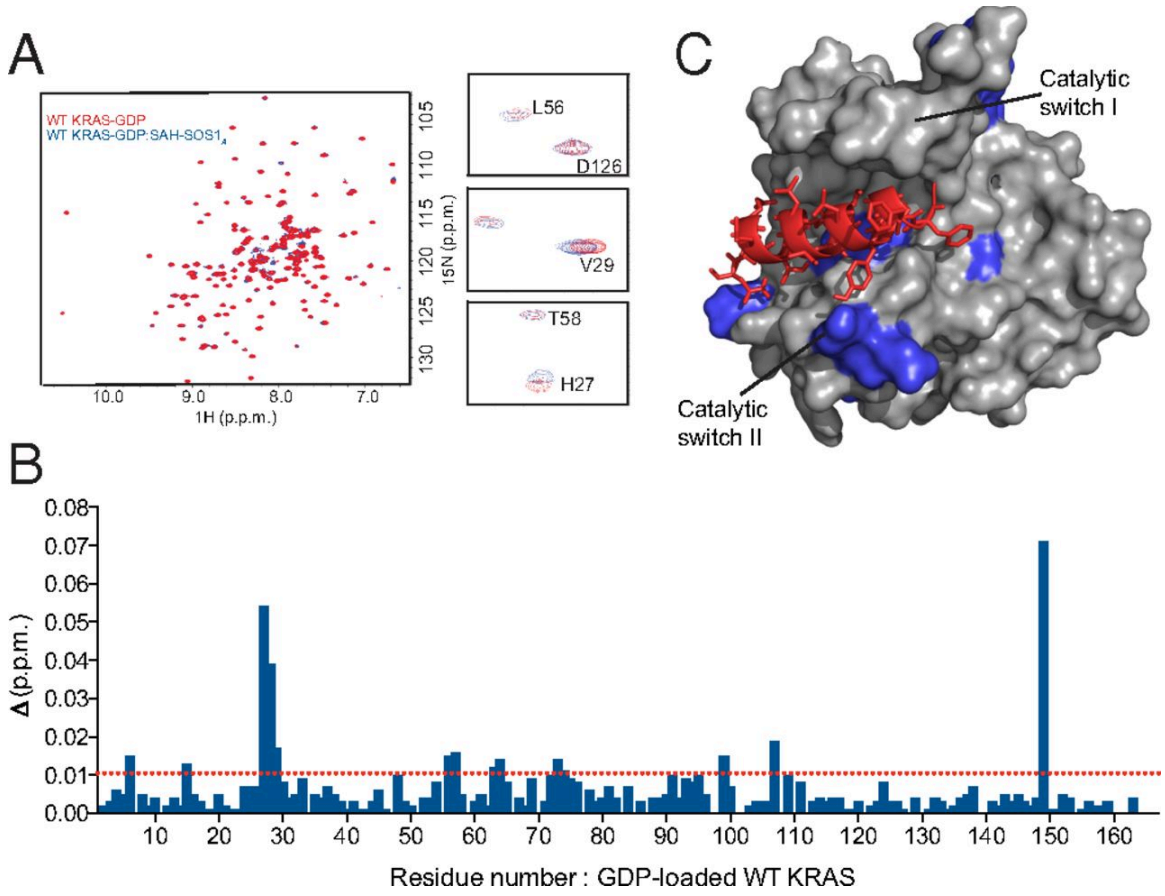

Figure 2-5: NMR analysis of SAH-SOS1$_A$/KRAS interaction. (*A*) ^{1}H-^{15}N HSQC spectrum of uniformly ^{15}N-labeled GDP-loaded WT KRAS in the absence (red) or presence of SAH-SOS1$_A$ (blue). (*B*) Chemical shift changes (significance threshold > 0.01 ppm) are plotted as a function of WT KRAS residue number. (*C*) SAH-SOS1$_A$ was docked onto KRAS (starting structural model PDB ID code 1NVU; HADDOCK software) based on HSQC data. The calculated model structure depicts the SOS1 helix engaging the SOS1-binding pocket of KRAS. Figure adapted from Leshchiner *et al*. (81).

2.4. Conclusions and future work

The studies in this section explore the biochemical and biophysical properties of stapled peptides. In particular, two related BIM peptides and their respective stapled versions were used to demonstrate the improved serum stability, helicity, and binding affinity of the stapled versions relative to the unstapled forms. While the magnitude of this change varied depending on the target of interest, it is clear that at least in select cases, stapling can improve the pharmacokinetic and pharmacodynamics properties of a peptide therapeutic. The stapled SOS1

peptide provides an instructive example where the addition of a hydrocarbon staple does not change the site of binding, but allows for improved affinity and biochemical properties.

Further work remains to explore the optimal charge, hydrophobicity, and staple location for any given peptide sequence (93). While some general principles have been elucidated for stapled peptide function, it is likely that every individual case will require the synthesis of a small library of stapled peptides which differ in these properties. There will likely be circumstances, particularly those when a native peptide sequence is already of very high affinity, when all possible staple positions prove deleterious, but in many other cases hydrocarbon stapling may present a relatively facile means for modifying a native peptide into a potentially useful tool compound.

3. Allosteric inhibition of anti-apoptotic MCL-1

3.1. Background

MCL-1 is one of the top ten most widely expressed pathologic factors in human cancers (26). Ongoing work in the Walensky lab has focused on disarming this potent cell survival protein. In 2010, the lab conducted a screen of all human BH3 domains in an attempt to find a peptide sequence selective for MCL-1 relative to all other apoptotic proteins. Surprisingly, the BH3 helix of MCL-1 itself was found to be the most selective binder to the canonical pocket of MCL-1 (65), a result which led to the synthesis of a stapled MCL-1 BH3 helix with improved properties relative to the native sequence. This stapled helix was then used in a competitive screen with more than 70,000 compounds to identify small molecules which bind selectively the MCL-1 BH3 pocket and not that of the related BCL-X_L (49). One molecule, termed MCL-1 inhibitory molecule 1 (MIM1) was extensively characterized in biochemical tests and found to bind directly to the canonical BH3 pocket of MCL-1 with minimal activity against other BCL-2 family proteins.

Interestingly, some molecules were found in the screen that retained inhibitory activity even when the protein-ligand complex was diluted (Figure 3-1). This implied that the molecules may be acting via in irreversible covalent mechanism, which has not been previously reported for MCL-1. Given this intriguing result the possible mechanism of this class of molecules was further explored.

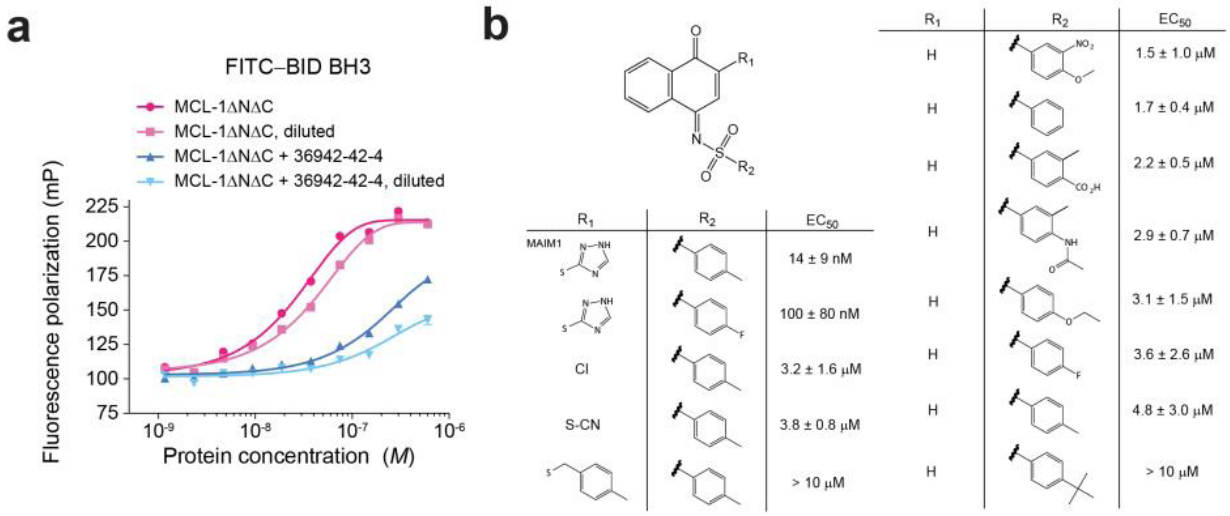

Figure 3-1: FITC−BID BH3 and MCL-1ΔNΔC in the presence and absence of N-(4-hydroxy-1-naphthalenyl)-benzenesulfonamide, a small molecule screening hit that exhibited irreversible inhibition of the BH3-binding activity of MCL-1ΔNΔC. (b) Chemical structures of MAIM1 analogs that emerged from the competitive MCL-1 $SAHB_A$−MCL-1ΔNΔC screen. Competitive potency corresponded to compound reactivity, based on the nature of the leaving group (R_1) and electron withdrawing capacity (R_2). Data are mean ± s.e.m. (n = 3 technical replicates). Data from Walensky lab 2012 screen (49). Figure adapted from Lee et al. (94).

3.2. Methods

3.2.1. Small-molecule characterization and synthesis.

MAIM1, *N*-(3-((1H-1,2,4-triazol-3-yl)thio)-4-oxonaphthalen-1(4H)-ylidene)-4-methylbenzenesulfonamide, was purchased from Vitas-M Labs (STK 215536) and resynthesized (*vide infra*) by established methods (95). 2-chloro-1,4-naphthoquinone (CAS 1010-60-2) was purchased from Santa Cruz Biotechnology, and all other reagents for the synthesis were purchased from Sigma-Aldrich. Proton (^{1}H) NMR spectra were acquired at 500 MHz on a Bruker Avance III instrument outfitted with a BBFO room-temperature probe. ^{1}H frequencies are referenced to TMS based on internal solvent signals. Proton spectra were acquired with a 45° pulse and a 4.3-s recycle delay at 0.3 Hz per point resolution.

3.2.2. N-(3-chloro-4-oxonaphthalen-1(4H)-ylidene)-4-methylbenzene sulfonamide (1).

2-chloro-1,4-naphthoquinone (1 mmol, 193 mg), 4-methylbenzene sulfonamide (1 mmol, 171 mg) and trimethylamine (2.2 mmol, 300 μL) were added to a flame-dried, purged microwave reactor tube at 0 °C. Anhydrous dichloromethane was added to a final volume of 8 mL, and this was followed by addition of 2 mmol $TiCl_4$ (2 mL of a 1 M solution in dicholormethane (DCM)), at which point the solution turned black and was heated to 60 °C in a microwave reactor (CEM Discovery) for 30 min. The mixture was poured into ethyl acetate (40 mL), and the insoluble black material was removed by filtration. The filtrate was concentrated under vacuum and resuspended in 30 mL DCM, the suspension was filtered, and the filtrate was concentrated. The resulting residue was suspended in 5 mL of 1:1 hexane/ethyl acetate, and the solid was isolated by filtration and washed with 1:1 hexane/ethyl acetate, thus yielding 58 mg of brown powder. R_f = 0.4 (TLC, 1:2 hexane/ethyl acetate); ^{1}H NMR (500 MHz, DMSO-d_6): δ = 8.44 (s, 1H), 8.09 (ddd, *J* = 1.1, 7.8, 11.3 Hz, 2H), 7.96 (d, *J* = 8.2 Hz, 2H), 7.90 – 7.78 (m, 2H), 7.52 (d, *J* = 8.2 Hz, 2H), 2.41 (s, 3H). HRMS (ESI^+): calculated for $C_{17}H_{12}ClNO_3S$ $(M+H)^+$ 346.03047, found 346.0299.

3.2.3. N-(3-((1H-1,2,4-triazol-3-yl)thio)-4-oxonaphthalen-1(4H)-ylidene)-4-methylbenzenesulfonamide (MAIM1; 2).

A solution of 9 mg of 1*H*-1,2,4-triazole-3-thiol in 2.5 mL tetrahydrofuran (THF) was added to a solution of 30 mg of **1** in 2.5 mL DCM. The solution was stirred at room temperature, and a brown precipitate formed. After 4 h, the solution was concentrated, and the resulting residue was suspended in 2 mL DCM and cooled to 0 °C. 2 mL of ice-cold hexane was then added, and a yellow-orange precipitate formed. This precipitate was isolated by

filtration and then washed three times with 1:1 DCM/hexane at 0 °C, thus yielding 15 mg of a yellow precipitate. R_f = 0.4 (TLC, 1:1 hexane/ethyl acetate); ^{1}H NMR (500 MHz, DMSO-d_6) δ = 9.83 (s, 1H), 9.01 (s, 1H), 8.57 (s, 1H), 8.11–8.02 (m, 2H), 7.87–7.74 (m, 3H), 7.53–7.42 (m, 3H), 2.41 (s, 3H). HRMS (ESI^+): calculated for $C_{19}H_{14}N^4O_3S^2$ $(M+H)^+$ 411.0580, found 411.0570.

3.2.4. Fluorescence polarization binding studies

Direct and competitive FP assays were performed as previously described (49). Direct binding curves were generated by incubating serial dilutions of protein with FITC–BID BH3 (15–60 nM) in 96-well format, and plates were read at equilibrium with a SpectraMax M5 microplate reader (Molecular Devices). For competitive FP assays, serially diluted small-molecule solutions were incubated with proteins at the indicated concentrations for 20 min at room temperature. FITC–BID BH3 was then added to the wells at the indicated concentrations, and the plates were read at equilibrium. Conjugation reactions were performed at room temperature for 45 min, and this was followed by removal of excess small molecules with spin columns (Bio-Rad) or overnight dialysis into FPLC buffer (150 mM NaCl and 50 mM Tris, pH 7.4). Data were analyzed by nonlinear regression analysis with Prism software (GraphPad).

3.2.5. Intact-protein mass spectrometry.

Proteins were analyzed on either a Waters LCT Premier^{XE} or Xevo mass spectrometer with a house-packed POROS trap for desalting. Protein spectra were averaged and deconvoluted with MagTran. All samples were compared to a myoglobin standard run on the same day.

3.2.6. Hydrogen/deuterium-exchange mass spectrometry

Deuterium labeling was initiated with an 18-fold dilution into D_2O buffer (150 mM NaCl and 50 mM Tris, pD 7.4) of a preequilibrated (20 min, room temperature) aliquot of each protein, peptide, and protein–peptide stock solution. At the indicated time points, the labeling reaction was quenched with the addition of an equal volume of quench buffer (150 mM potassium phosphate, pH 2.5). Each deuterium labeling experiment was performed in at least duplicate. The error of determining the average deuterium incorporation for each peptide was at or below ±0.25 Da. Relative deuterium levels for each peptide were calculated by subtracting the average mass of the undeuterated control sample from that of the deuterium-labeled sample. All mass spectra were processed with DynamX 3.0 (Waters Corporation).

3.2.7. Molecular dynamics calculations

Protein Setup:

The NMR structure of apo MCL-1 (PDB ID: 2MHS) was used for all calculations (33). The hexa-histidine tag was deleted and Ser 286 was computationally mutated to Cys or Trp using Maestro. The protein was prepared for calculations using the default parameters of the Protein Preparation Workflow in Maestro (96). Protonation states were those predicted to occur at pH 7.0 using the Epik module (97). For calculations of the MCL-1/MIMX complex, the MIMX small molecule was built using Meastro and a covalent bond to Cys 286 was manually added.

Molecular Dynamics System Setup:

Each protein was pre-soaked in a cubic box of TIP3P water molecules using the System Builder workflow in Desmond (98). The box was sized to leave all peptide atoms at least 1 nm from the boundaries. All overlapping solvent molecules were removed, the system was charge

neutralized with appropriate counterions, and 150 mM NaCl was added to simulate buffer conditions.

Molecular Dynamics Simulations:

All MD simulations were performed using the Desmond package, with the OPLS-AA 2005 forcefield used to model all interactions (99). Periodic boundary conditions were maintained throughout. Long-range electrostatic interactions were calculated using the particle-mesh Ewald method (100), and van der Waals and short-range electrostatic interactions were smoothly truncated at 0.9 nm. Constant system temperature of 300 K was maintained using Nose-Hoover thermostats (101), and system pressure was maintained at 1 atm using the Martina-Tobias-Klein method (102). The equations of motion were integrated using the RESPA integrator (103), with a 2.0 fs timestep for bonded and short-range interactions and a 6.0 fs timestep for non-bonded interactions beyond the 0.9 nm cutoff. The default parameters in Desmond were used to relax the system prior to simulation (104). Following this, a 100 ns production simulation was run and configurations saved at 4 ps intervals. All simulations were judged to have converged on the basis of radius of gyration calculations and RMSD.

3.3. Results and discussion

3.3.1. Chemical properties and synthesis of MAIM1

The compounds identified as possible covalent inhibitors from the chemical screen are naphthoquinone arylsulfonimines, which are known highly reactive molecules. Indeed, the activity of the molecules in the screen correlates closely with their electrophilicity (Figure 3-1B), implying that nucleophilic addition of the protein into the molecule is the likely mechanism of action. The most potent of the molecules, termed MCL-1 allosteric inhibitory molecule 1 (MAIM1), features numerous reactive chemotypes (Figure 3-2). These include an

activated α,β-unsaturated carbonyl moiety which is a possible site for nucleophilic addition as well as multiple unstable linkages and a location for possible redox cycling. Such reactive molecules have been dubbed pan-assay interference compounds or PAINS (105), and are generally viewed as unreliable starting points for drug discovery efforts. In this case although highly reactive, MAIM1 was still selective for MCL-1 over BCL-X_L, implying that its activity may be tunable to different BCL-2 family members. Moreover, a covalent ligand binding to MCL-1 presents a new mechanism of action that has not been explored.

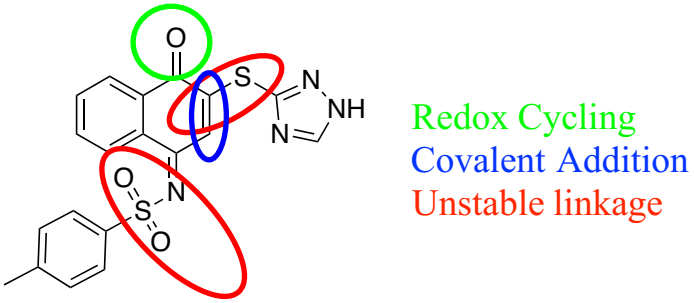

Figure 3-2: The structure of MAIM1, featuring numerous reactive functionalities characteristic of PAINS.

MAIM1 is available commercially, but not in a highly pure form, likely due to the overall reactivity of the molecule and its numerous possible sites of degradation. As a result, it was resynthesized for further testing. The synthesis of related hydronapthoquinones has been reported (95), and synthesis of MAIM1 proceeded using similar methods (Figure 3-3).

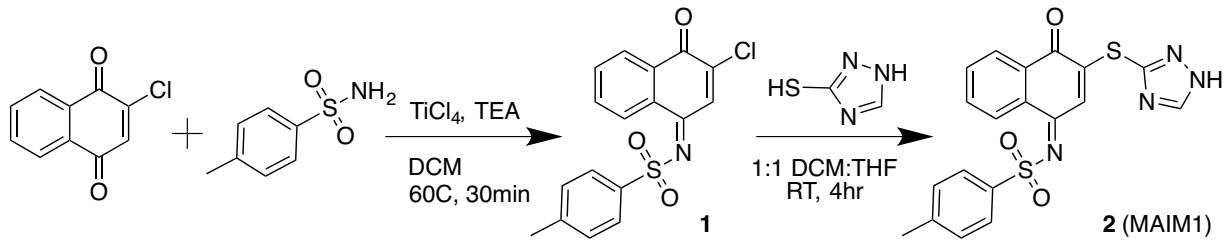

Figure 3-3: Synthesis of MAIM1

Synthesis begins with a Lewis-acid mediated coupling of a sulfonamide to commercially-available 2-chloro-1,4-naphthoquinone using microwave heating. The product **1** was purified by trituration of the solid formed. This was then substituted with the nucleophilic 1H-1,2,4-

triazole-3-thiol to yield solid MAIM1. The final product was purified by trituration with DCM and hexane. Consistent with the known reactivity of the molecule, it was unstable, and was stored under an atmosphere of argon in the dark at -20 degrees Celsius to minimize degradation. Attempts to HPLC the molecule were unsuccessful due to degradation on the column.

3.3.2. MAIM1 covalently modifies MCL-1 at C286

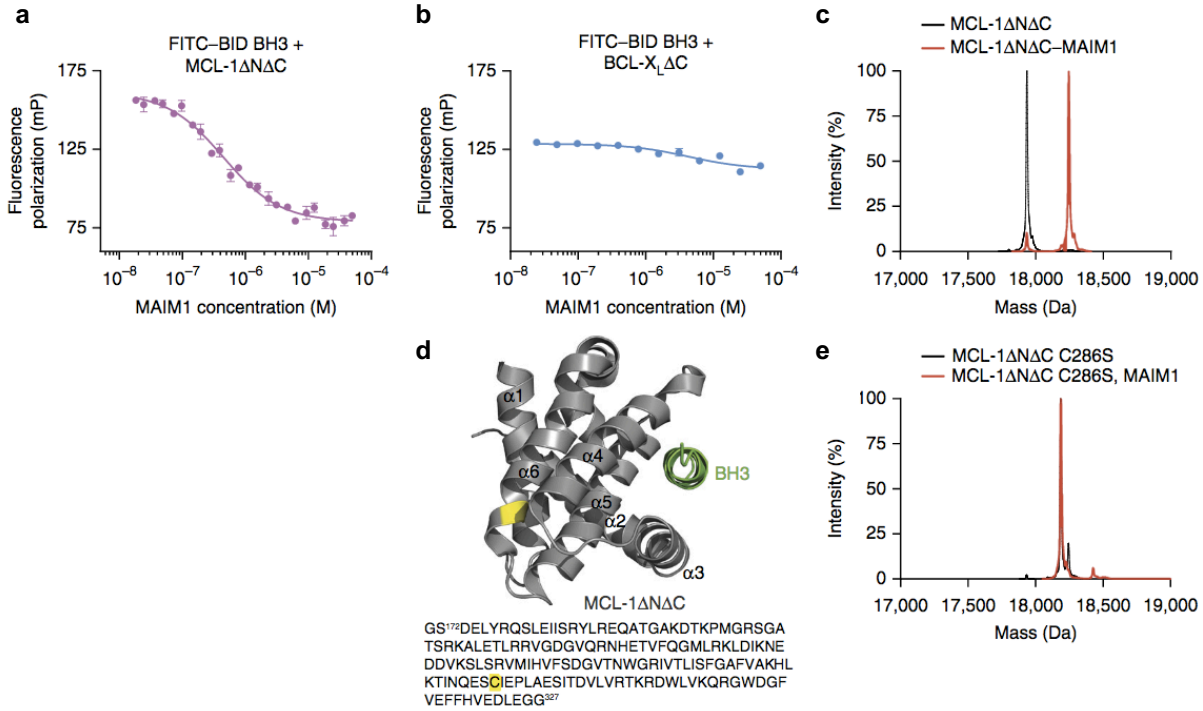

Figure 3-4: MAIM1 selectively modifies MCL-1 by covalent attachment to C286. (a) FP competitive binding assay for MAIM1 inhibition (half-maximal inhibitory concentration, 450 nM) of the interaction between FITC–BID BH3 (15 nM) and MCL-1ΔNΔC (125 nM). Data are shown as mean ± s.e.m. (n = 3 technical replicates). (b) Negative-control FP assay for MAIM1, as tested on the binding interaction between FITC–BID BH3 (15 nM) and BCL-X_LΔC (125 nM). (c) Intact-protein MS of MCL-1ΔNΔC (black, 17,937 Da) and MAIM1-derivatized (naphthoquinone tosylimine) MCL-1ΔNΔC (red, 18,247 Da). (d) MAIM1 derivatization of MCL-1ΔNΔC C286 (yellow), as determined by MS/MS analysis. The location of the BH3-binding groove is demonstrated by MCL-1 $SAHB_D$ (green) (PDB 3MK8) (e) Intact-protein MS of MCL-1ΔNΔC C286S alone (black, 18,191 Da) and in the presence of MAIM1 (red, 18,191 Da), showing overlapping peaks (red trace obscures underlying black trace). Data for panels c-e from the DFCI mass spectrometry core and S. Lee, PhD. Figure adapted from Lee *et al*. (94).

Competitive fluorescence polarization assays were conducted in order to assess the functional effects of conjugation with MAIM1. In these assays, the small molecule is tested for

its ability to prevent binding of a BH3 ligand, in this case that of the protein BID. MAIM1 was pre-incubated with either MCL-1ΔNΔC (Figure 3-4A) or BCL-X_LΔC (Figure 3-4B) before addition of BID-BH3. In this assay, MAIM1 has a clear dose-dependent inhibitory effect for binding to MCL-1 (half-maximal inhibitory concentration, 450 nM), but not BCL-X_LΔC.

Intact protein mass spectrometry indicates that MAIM1 covalently labels MCL-1ΔNΔC (Figure 3-4C). Further MS/MS analysis localizes the covalent binding site to C286, localized on the opposite surface of the protein as the canonical binding pocket (Figure 3-4D). To validate the requirement of C286 for MAIM1 activity, intact protein mass spectrometry was repeated with the mutant protein MCL-1ΔNΔC C286S, indicating that this mutation abrogates MAIM1 conjugation (Figure 3-4E).

3.3.3. MAIM1 impairs the capacity of MCL-1ΔNΔC to protect BID BH3 from deuterium exchange

To further interrogate the structural mechanism of how MAIM1 modifies the BH3 binding capacity of MCL-1ΔNΔC, the peptide was examined using hydrogen/deuterium-exchange mass spectrometry (HXMS). In this technique, a peptide is transferred from a buffer containing water to one containing heavy water (D_2O). Any hydrogen atoms in the sample that are exchangeable with solution will then incorporate a deuterium label, thus increasing the mass of the peptide. Changes in peptide structure affect the rate of this exchange by modifying the solvent accessibility of the peptide hydrogens. For instance, if a helical structure is stabilized the rate of H/D exchange will tend to decrease as the protons spend relatively more time in stable hydrogen bonds rather than free in solution (106).

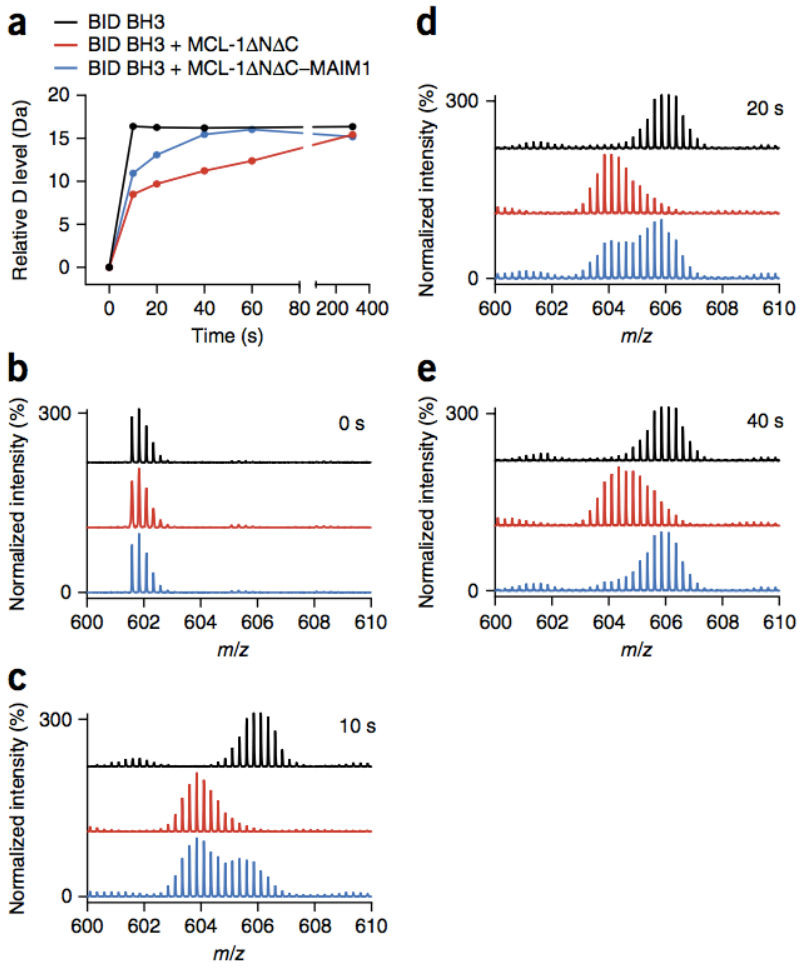

Figure 3-5: Exchange of BH3 peptide amide hydrogen for deuterium measured by mass spectrometry. (a) Deuterium (D)-exchange time course for BID BH3 alone (black) or in the presence of MCL-1ΔNΔC (red) or MAIM1-derivatized MCL-1ΔNΔC (blue). (b–e) MS spectra of BID BH3 peptide at 0 (b), 10 (c), 20 (d) and 40 s (e) for each experimental condition. HXMS data from the Engen Lab at Northeastern University. Figure adapted from Lee *et al*. (94).

The deuterium-exchange profile of a BID BH3 peptide was examined alone, in the presence of MCL-1ΔNΔC, and the presence of MCL-1ΔNΔC conjugated to MAIM1 (Figure 3-5). BID BH3 alone underwent rapid and complete deuterium exchange within 10 s of dilution into deuterium buffer, a result consistent with its disordered structure in solution. However in the presence of added MCL-1ΔNΔC, deuterium exchange was markedly slowed, reflecting induced folding and ligand-target interaction. After MAIM1 conjugation the inhibitory effect of MCL-1ΔNΔC on BID BH3 deuterium exchange was impaired, as evidenced by more rapid deuteration. Whereas one peptide subpopulation was initially protected (as in the presence of

MCL-1ΔNΔC), the other portion was rapidly deuterated, and complete exchange was restored by the 40-s time point. These data indicate that MAIM1 derivatization of MCL-1ΔNΔC drives the BH3 binding equilibrium to the unbound state.

3.3.4. MAIM1 conjugation reduces conformational flexibility of MCL-1 in molecular dynamics simulations

The site of MAIM1 conjugation is physically quite distinct from the canonical BH3 binding pocket, yet addition of a small molecule at that location significantly reduces the ability of MCL-1 to bind a BH3 helix. The conformational mechanism for this finding was explored using molecular dynamics (MD) simulations. These calculations are classical, as opposed to quantum mechanical, in origin, and model the protein as a series of point charges. A forcefield, which incorporates terms for all of the covalently bonded and non-bonded interactions between the particles, is used to evaluate the energies of a particular conformation (99). The dynamic properties of the system are then modeled by solving Newton's equations of motion over very short timescales comparable in time to the vibration of a chemical bond (femtoseconds). By iteratively solving Newton's equations over millions to billions of these short steps, the behavior of the system can be modeled over timescales approaching 1 microsecond. The overall properties of the system are then calculated using statistical mechanics to give a description of the ensemble. One key parameter describing the simulations is the calculated root mean square fluctuation (RMSF) of each reside, which measures the average amount of motion of the Cα during the course of the simulation. Greater relative RMSF between liganded and unliganded forms of a protein indicates increased motion during the course of the simulation, implying a destabilization of part of the structure. In contrast, reduced RMSF is indicative of increased conformational stability.

Simulations were conducted to model the motion of MCL-1 protein in the presence and absence of MAIM1 derivitzation at C286 (Figure 3-6). The calculations suggest a decrease in the flexibility of MCL-1 protein in two discrete regions, including the otherwise mobile N terminus and, most intriguing, the region including α4 and portions of the adjacent α5 and α3 helices, which bridges the C286 region of α6 and the canonical groove at the opposite face of the protein (Figure 3-6A-B).

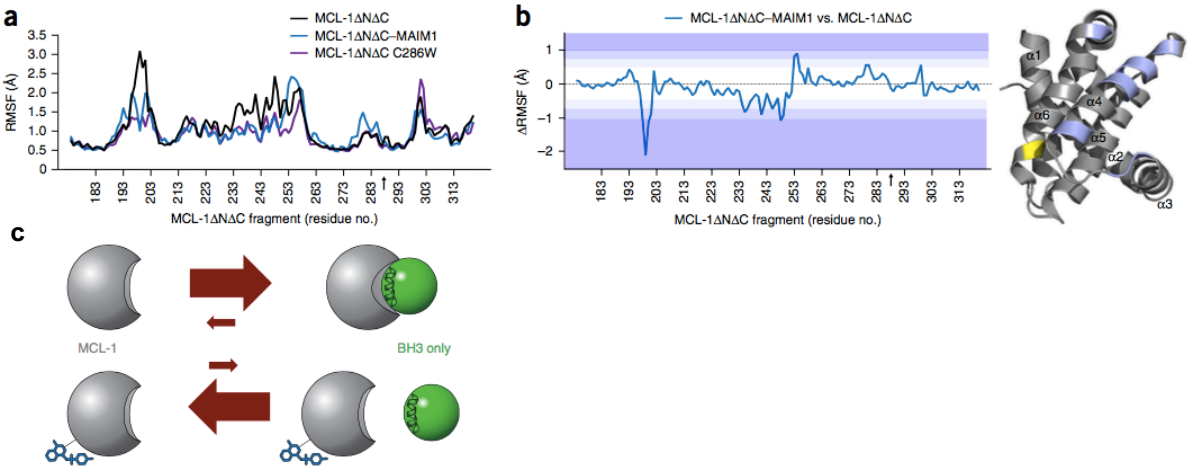

Figure 3-6: Results of molecular dynamics simulations of MCL-1 in the presence and absence of MAIM1 derivitization. (a) Comparative r.m.s. fluctuations (RMSF) of backbone atoms for MCL-1ΔNΔC (black), MAIM1-derivatized MCL-1ΔNΔC (blue) and MCL-1ΔNΔC C286W (purple). The black arrow on the *x* axis indicates the C286 position. (b,c) Difference plots for MCL-1ΔNΔC−MAIM1 minus MCL-1ΔNΔC (b) and MCL-1ΔNΔC. Color shading corresponds to changes in the RMSF of 1 s.d. (light purple), 1.5 s.d. (purple) and >2 s.d. (dark purple) from the mean differences. A region of decreased mobility that includes portions of α4 and the adjacent α5 and α3 helices, which bridge the C286 region of α6 and the canonical BH3-binding groove, is highlighted on the structure of MCL-1ΔNΔC (PDB 3MK8) according to the corresponding color scale. The position of residue 286 is indicated by a black arrow on the *x* axis and is colored yellow on the structure. (c) Model for allosteric inhibition of MCL-1. Upon interaction with the canonical groove of MCL-1, BH3 domains undergo induced α-helical folding, and the protein conformationally adapts to BH3 engagement, thus yielding a high-affinity interaction. Figure adapted from Lee *et al*. (94).

Conformational flexibility of the canonical groove has been implicated in induced α-helical folding of BH3 domains and protein adaptation to maximize binding contacts with α-helical peptides and small-molecule inhibitors (107,108). Whereas a shallow groove at the N-terminal face of proapoptotic BAX is more readily bound by a prefolded stapled α-helix, the deeper groove at the C-terminal pockets of BAX and other BCL-2 family proteins is capable of

binding peptides that are otherwise linear in solution but fold after groove engagement (39,109). Thus, a structure–function model that incorporating these results predicts that MAIM1 derivatization rigidifies the MCL-1 structure in a manner that prevents conformational adaptation of the C-terminal groove to BH3 ligands and thereby decreases the BH3 binding efficiency and functional activity of MCL-1 (Figure 3-6C).

3.4. Conclusions and future work

MCL-1 remains a critical cancer target that so far remains undrugged. This work opens a new potential mechanism for disarming MCL-1 by targeting an allosteric site distant from the canonical BH3 binding groove that has been the target of all existing drug discovery efforts. HXMS studies indicate that alteration of the C286 region of MCL-1 allosterically impairs the capacity of the canonical groove to engage BH3 domains, thus resulting in functional suppression of the antiapoptotic binding activity implicated in oncogenesis and chemoresistance. Moreover, this mechanism appears to decrease MCL-1's BH3 binding efficiency rather than to block it entirely, a potentially desirable outcome given the toxicities associated with complete MCL-1 deletion. By shifting the BH3 binding equilibrium from a predominantly MCL-1-bound state to an unbound state, allosteric inhibitors of this noncanonical C286 site may provide a new opportunity for therapeutic targeting of MCL-1 in cancer.

The present MAIM1 molecule with its poor stability and reactive functional groups is not a tractable chemical probe. Future work must identify a more stable electrophile with sufficient reactivity to bind C286 but without the undesirable features of MAIM1. Such a molecule would allow for further exploration of the functional role of this allosteric site, and would permit more conclusive determination of the utility of drugging this position. Tools for

computational evaluation of covalent ligands have been developed (110), and new screening efforts specifically seek allosteric covalent binders (111). It remains to be determined whether a better molecule than MAIM1 can be developed, but such a compound could be an important new therapeutic angle in the range of malignancies that overexpress MCL-1.

4. A fragment ligand sensitizes BAX to activation by BH3 ligands

4.1. Background: fragment-based screening

BAX is among the key effector proteins in apoptosis, and permeabilizes the outer mitochondrial membrane to release cytochrome C and activate downstream apoptotic effectors (38). It is thus one of the key regulatory points in apoptosis, and so the interplay between cellular life and death depends heavily on the activation or sequestering of BAX. A small molecule regulator of BAX would thus have the potential to greatly influence cell fate. Among strategies to look for new chemical matter, fragment-based screening is emerging as a powerful discovery tool (112). In this technique, a small library generally containing no more than a few thousand unusually small molecules (MW < 250 daltons) is screened against the target of interest. By remaining small and relatively unfunctionalized, this library can span a relatively large range of chemical space with many fewer members than in typical ligand-based screens. The tradeoff is that each compound is likely to have very weak affinity for the target, requiring significant medicinal chemistry to optimize the fragment once a hit is identified. Likewise, very sensitive hit detection methods must be used to detect the weak binding energies typical of fragments. Despite these drawbacks, fragment-based screening was used by AbbVie Inc. to discover the small molecule ABT-737 (25), the precursor molecule to the first FDA-approved BCL-2 inhibitor Venetoclax (22).

Nuclear magnetic resonance offers the sensitivity required to detect weak binding, but suffers from low throughput and a requirement for large amounts of pure protein. Additionally, NMR is very sensitive to inhomogeneity in sample, requiring a consistent, uniform protein preparation throughout a screen. In January of 2015, the Harvard Medical School NMR Core purchased the Maybridge Collection of approximately 1,000 fragments in a format for high-

throughput screening. Given the critical importance of BAX in cell death, it was decided to leverage this new capability to conduct the first ever fragment screen against this protein.

4.2. Methods

4.2.1. Expression and purification of monomeric full-length BAX

Recombinant, full-length BAX was expressed in BL21 (DE3) *E. coli* using the pTYB1 vector. Cell pellets were resuspended in 20 mM Tris, 250 mM NaCl, pH 7.2 and lysed by two passes through a microfluidizer (Microfluidics) chilled to 4°C. The lysate was clarified by centrifugation at 20,000 rpm. BAX was purified by batch affinity binding at 4°C using chitin resin (New England Biolabs), followed by loading onto gravity flow columns for washing and elution. The intein-chitin binding domain tag was cleaved by 36 hour incubation in 50 mM dithiothreitol at 4°C. Pure protein was isolated by size exclusion chromatography (Superdex 75 10/300; 20 mM potassium phosphate, pH 6.2) using an FPLC system (GE Healthcare Life Sciences).

4.2.2. Fragment screening by STD-NMR

The Ro3 diversity fragment library was purchased from Maybridge, and molecular fragments characterized by ^{1}H-NMR and then pooled in groups of 10 to minimize spectral overlap. Forty fragments were excluded prior to screening as part of a quality control measure that identifies poorly-behaved fragments. Fragment pools were added to a 5 μM solution of unlabeled, full-length human BAX in 20 mM potassium phosphate buffer, pH 6.2 in 10% D_2O, resulting in a final compound concentration of 300 μM. The mixing and loading of samples into a 5-mm NMR tube was performed using a liquid handling robot (Gilson). STD-NMR measurements were acquired at 25°C on a Varian Inova 500-MHz spectrometer equipped with

a helium-cooled cryoprobe. Low power saturation of the protein was achieved with a series of 50 ms Gaussian pulses for a total of 3 seconds; on-resonance irradiation was performed at 0.8 ppm, and off-resonance irradiation at 30 ppm. Standard excitation sculpting was used for solvent suppression. Each experiment was run for 14 min. The results were initially analyzed by comparing the on and off resonance STD spectra for each pool to determine the presence of binders, with 37 out of 96 pools demonstrating evidence of protein interaction. Subsequently, each pool was analyzed to identify individual binders using in-house display analysis and display software, which allowed for precise alignment of on- and off-resonance spectra. Fragments in pools that yielded a positive STD signal were then subdivided into groups of three for retesting. Those fragments that exhibited STD in both experiments were reordered from Maybridge and tested both as single compounds and in competitive binding experiments.

4.2.3. Competition STD-NMR

Individual fragments were added to 5 μM BAX with or without 5 μM competitor peptide in 20 mM potassium phosphate buffer, pH 6.2. STD-NMR was measured as described above. Fragments that were competed by vMIA or BIM $SAHB_{A2}$ showed a decreased saturation-transfer difference in the presence of peptide relative to no peptide.

4.2.4. HSQC NMR

Uniformly ^{15}N-labeled recombinant BAX was generated as previously described (39,113). Protein samples with the indicated molar ratio of fragment were prepared in 25 mM sodium phosphate, 50 mM NaCl solution at pH 6.0 in 10% D_2O. Correlation ^{1}H-^{15}N HSQC spectra were acquired at 25°C on a Bruker 600 MHz NMR spectrometer equipped with a cryogenic probe, processed in Topspin (Bruker) and analyzed using CcpNmr Analysis. The

weighted average chemical shift difference was calculated as $Shift = \sqrt{0.5 \times [\delta_H^2 + (\alpha \times \delta_N^2)]}$, where ΔH/ΔN is the change in p.p.m. of ^{1}H or ^{15}N for the indicated crosspeak. The scale factor 0.2 was used to compare ^{1}H or ^{15}N peaks. The absence of a bar indicates no chemical shift difference, or the presence of a proline or residue that is overlapped or not assigned. BAX cross-peak assignments were applied as previously reported (38). The significance threshold for the chemical shift changes was calculated based on the average chemical shift across all residues plus the standard deviation, in accordance with standard methods.

4.2.5. Liposomal release assay

Large unilamellar vesicles (LUVs) with a lipid composition similar to the outer mitochondrial membrane were formed by liposome extrusion as previously described[38,41]. Briefly, a lipid mixture containing a 48:28:10:10:4 molar ratio of phosphatidylcholine, phosphatidylethanolamine, phosphatidylinositol, dioleoyl phosphatidylserine, and tetraoleolyl cardiolipin in chloroform (Avanti Polar Lipids) was generated and lipid films formed by evaporation of solvent, initially under nitrogen gas and then by overnight vacuum, followed by storage at -80 °C under nitrogen. Lipid films were hydrated in 1 mL assay buffer (10 mM HEPES, 200 mM KCl, 1 mM $MgCl_2$, pH 7.0) and mixed with the fluorophore and quencher pair, 8-aminonaphthalene-1,3,6-trisulfonic acid (ANTS, 12.5 mM) and p-xylene-bis-pyridinium bromide (DPX, 45 mM). Liposomes were formed by 5 freeze/thaw cycles followed by extrusion through a 100 nm polycarbonate membrane and purified using a Sepharose CL-2B size-exclusion column. For measurement of BAX activation, BAX (750 nM) was added to the indicated concentration of molecular fragment in the presence of liposomes, followed by BIM $SAHB_{A2}$ (750 nM), at the indicated time points. The assay was carried out in black opaque 384 well plates (30 μl per well). ANTS/DPX release was monitored over time at room temperature

in a spectrofluorometer (Tecan Infinite M1000) using an excitation wavelength of 355 nm, an emission wavelength of 540 nm, and a bandwidth of 20 nm. Maximal release was determined by the addition of Triton X-100 to a final concentration of 0.2% (v/v). Percent release was calculated as ((F−F0)/(F100−F0)) ×100, where F is the observed release, and F0 and F100 are baseline and maximal fluorescence, respectively.

4.2.6. Fluorescence polarization assay

FITC-peptide (25 nM) was incubated with a serial dilution of recombinant, full-length BAX in binding buffer (20 mM Potassium phosphate, pH 6.2). For competitive FP, FITC-peptide (25 nM) was mixed with a fixed concentration of BAX (250 nM) and incubated with a serial dilution of acetylated peptide or molecular fragment. Fluorescence polarization was measured at equilibrium using a SpectraMax M5 microplate reader. Nonlinear regression analysis of dose-response curves was performed using Prism software 7 (GraphPad).

4.2.7. Docking calculations

The Schrodinger software suite (Version 2016-2) was used throughout. Conformations of molecule BIF-44 were generated in MacroModel using the OPLS3 forcefield (114). Each of the 20 NMR conformations of Bax (PDB:1F16) was separately prepared using the default parameters in the PrepWiz wizard in Maestro. The docking receptor grid (radius 1 nm) was defined at the center of Ala124, the amino acid with the greatest HSQC shift. BIF-44 was then docked into all 20 structures using Glide Extra Precision (XP) mode (115). The top-scoring poses were then manually inspected for consistency with experimentally-determined HSQC shifts for the complex.

4.2.8. Molecular dynamics calculations

Protein Setup:

The first structure of Bax from 1F16 was used as the starting structure for the calculations. The protein was prepared for calculations using the default parameters of the Protein Preparation Workflow in Maestro (96). Protonation states were those predicted to occur at pH 7.0 using the Epik module (97).

Molecular Dynamics System Setup:

Each protein was pre-soaked in a cubic box of TIP3P water molecules using the System Builder workflow in Desmond (98). The box was sized to leave all peptide atoms at least 1 nm from the boundaries. All overlapping solvent molecules were removed, the system was charge neutralized with appropriate counterions and 150 mM NaCl was added to simulate buffer conditions.

Molecular Dynamics Simulations:

All MD simulations were performed using the Desmond package, with the OPLS3 forcefield used to model all interactions (114). Periodic boundary conditions were maintained throughout. Long-range electrostatic interactions were calculated using the particle-mesh Ewald method (100), and van der Waals and short-range electrostatic interactions were smoothly truncated at 0.9 nm. Constant system temperature of 300 K was maintained using Nose-Hoover thermostats (101), and system pressure was maintained at 1 atm using the Martina-Tobias-Klein method (102). The equations of motion were integrated using the RESPA integrator (103), with a 2.0 fs timestep for bonded and short-range interactions and a 6.0 fs timestep for non-bonded interactions beyond the 0.9 nm cutoff.

The default parameters in Desmond were used to relax the system prior to simulation (104). Following this, a 100 ns production simulation was run and configurations saved at 4 ps intervals. All simulations were judged to have converged on the basis of radius of gyration calculations and RMSD.

4.3. Results and discussion

4.3.1. NMR fragment screen of full-length BAX

To generate recombinant, full-length BAX of sufficient quantity and stability to execute a molecular fragment screen, production was scaled to an overall culture volume of 48 liters, and bacterial pellets were lysed using a temperature-controlled microfluidizer (set at 4^{o}C), followed by batch binding of the lysate to chitin affinity resin, dithithreitol (DTT) elution, and purification by size exclusion chromatography. Using this approach, 22 mg of BAX protein at a concentration of 0.64 mg/mL was generated for initial screening, representing an overall yield of 0.45 mg of pure, full-length protein per liter of bacterial culture.

The fragment screen was conducted using saturation transfer difference (STD) NMR to identify molecules that interact with BAX. STD-NMR measures the change in ^{1}H-NMR signal of a ligand following selective irradiation of the target protein, where transfer of magnetization from protein to ligand causes a decrease in signal that reflects ligand-protein interaction. This technique is sensitive to ligands even with weak (10^{-3} M) binding (116), has rapid acquisition time, relative ease of analysis, and the ability to pool compounds with non-overlapping ^{1}H-NMR spectra, making STD-NMR a tractable platform for advancing a fragment-based screen of pro-apoptotic BAX.

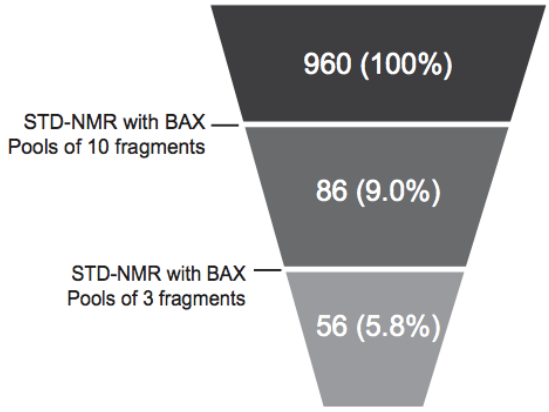

Figure 4-1: Identification of BAX-interacting fragments (BIFs) by sequential STD-NMR screening in pools of 10, 3, and then singlet, yielding 56 candidate BIFs. Figure adapted from Pritz *et al*. (accepted).

The Maybridge Ro3 library of 1000 molecular fragments was used for the BAX screen. The compounds were characterized by ^{1}H-NMR and pooled in groups of ten such that spectral overlap was minimized. Of the 96 pools analyzed, a positive STD signal was detected in 37, which represented 86 individual hits that were then rescreened in pools of three, ultimately yielding 56 confirmed interactors (Figure 4-1). Fifty-three commercially available fragments were ordered, retested by STD as singletons, and confirmed as BAX-Interacting Fragments (BIFs). Nearly half of the identified BIFs were composed of linked or fused five and six-membered rings (Figure 4-2).

4.3.2. BIF-44 sensitizes BAX to BH3-mediated activation

To determine if any of the identified BIFs influenced the function of BAX, the 53 BIFs were screened in a liposomal release assay. In this assay, a synthetic liposome is made which contains both a fluorescent dye and a quencher. When the liposome is intact, no fluorescence is observed as the dye is quenched by the close proximity to the quencher. The addition of activated BAX forms a pore in the liposome, causing dye release and increased fluorescence. This assay thus allows for identification of BAX activators and inhibitors. For this study, the assay was modified to also test for sensitizers of activation, meaning compounds that alone

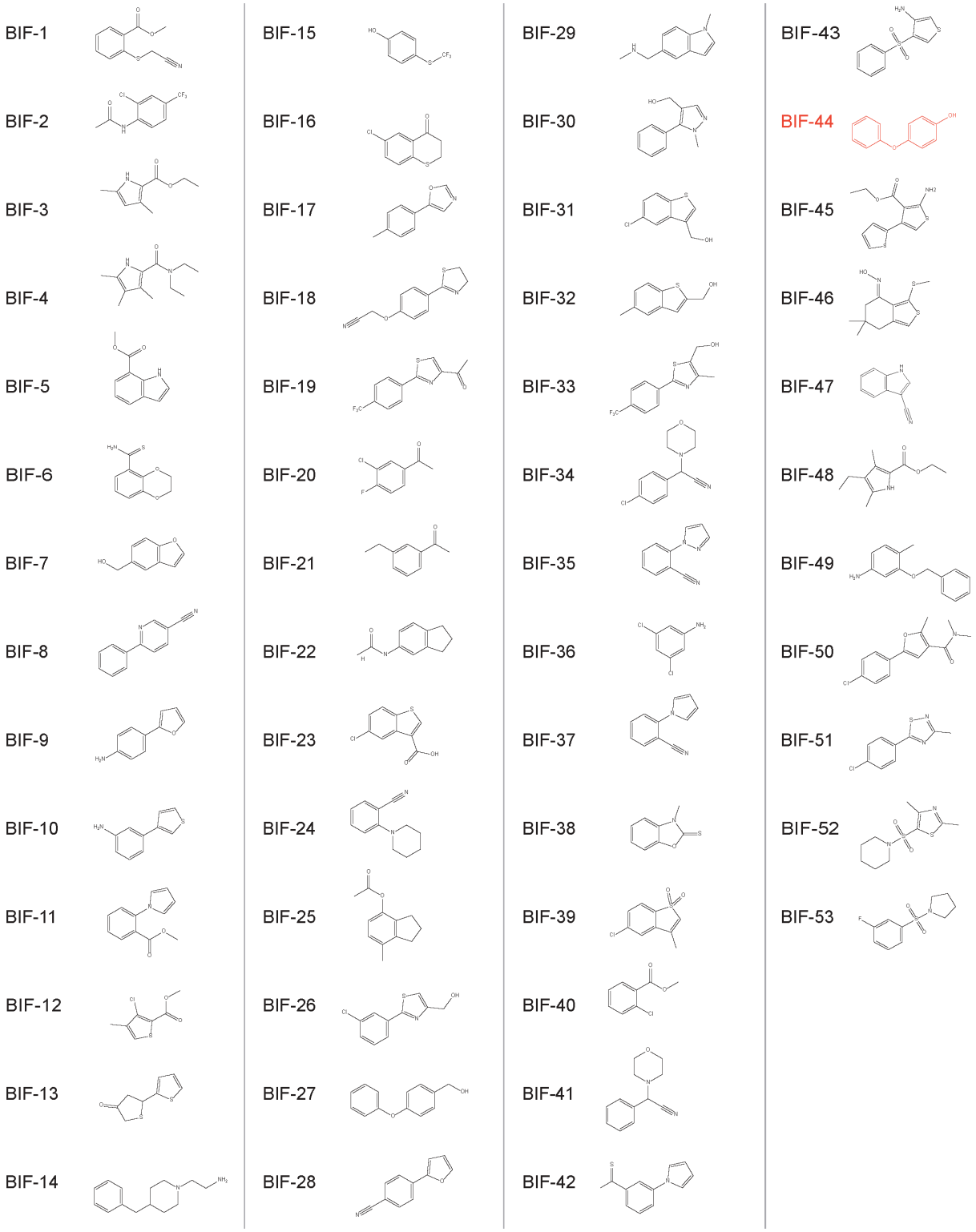

Figure 4-2: Molecular structures of the 53 fragments that bind to full-length BAX by STD NMR. Figure adapted from Pritz *et al*. (accepted).

only weakly activate BAX, but when combined with an activating BH3 peptide result in an enhancement of normal activation.

First, baseline fluorescence with liposomes and compound alone is read, followed by the addition of BAX to evaluate for direct activation; then, BIM SAHB$_{A2}$ (aa 145-164; (70)) is added to this mixture and the effect of the combination monitored, and compared with the triggering activity of BIM SAHB$_{A2}$ and BAX in the absence of compound. Using this assay format, 4 direct activators of BAX-mediated liposomal release and 8 sensitizers of BIM SAHB$_{A2}$-triggered BAX activation were identified from among the 53 BIFs. The direct activator profile is exemplified by the positive control BIM SAHB$_{A2}$ peptide, which induces time-responsive liposomal release in the presence of BAX alone (Figure 4-3; blue trace). The sensitizer profile is most strikingly reflected by the activity of BIF-44 (4-phenoxy-phenol). This molecule has a minimal effect on BAX when incubated as a single agent, but when combined with BIM SAHB$_{A2}$ the maximal BAX-mediated release jumped from 50% with BIM SAHB$_{A2}$ alone to 80% for the combination (Figure 4-3; red trace).

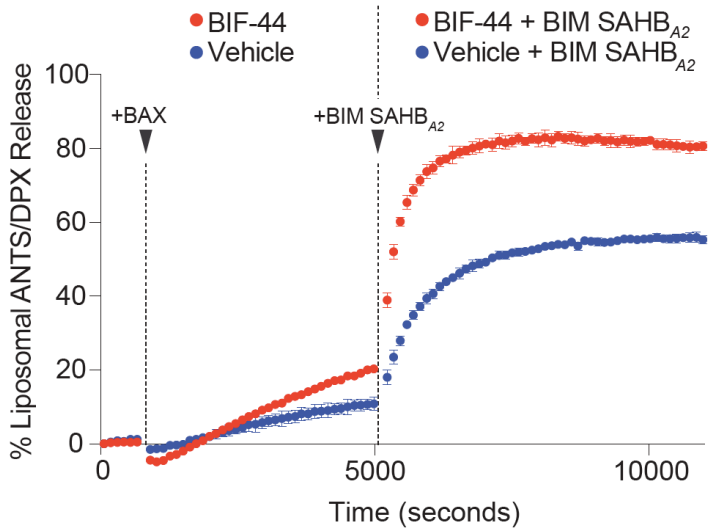

Figure 4-3: BIF-44 sensitizes BAX to activation by BIM SAHBA2. BIF-44 has no independent effect on the liposomes (red, left), minimal direct BAX activation activity (red, middle), but notably enhances the kinetics and quantity of liposomal release upon addition of BIM SAHBA2 (red, right), exceeding the maximal level of release achieved by the BIM SAHBA2 and BAX combination alone (blue, right). Error bars are mean ± SD for experiments performed in triplicate. Data from J. Pritz. Figure adapted from Pritz *et al*. (accepted).

4.3.3. BIF-44 competes with vMIA for BAX interaction

Multiple peptides bind to distinct regions of BAX with varying functional effects (Figure 1-3). In order to help localize the binding site for BIF-44 on BAX, a series of competitive binding experiments were performed using some of these peptides. BIM $SAHB_{A2}$ binds at the BH3-trigger site (39), while inhibitory vMIA binds to a distinct site on the opposite face of the protein. Both N-terminal acetylated BIM $SAHB_{A2}$ and BIF-44 were used to compete off the direct interaction between FITC-BIM $SAHB_{A2}$ and BAX (Figure 4-4A). Whereas Ac-BIM $SAHB_{A2}$ dose-responsively competed with FITC-BIM $SAHB_{A2}$ for BAX binding, BIF-44 had little to no effect. In contrast BIF-44 dose-responsively competes with FITC-vMIA for BAX interaction (Figure 4-4B). To confirm the competitive nature of the binding between vMIA and BIF-44, STD experiments were repeated with BIF-44 in the presence of both BAX and vMIA peptide (Figure 4-4C). BIF-44 demonstrates reduced STD signal upon co-incubation of the peptide, indicating that the peptide reduces small molecule binding, and thus spin transfer.

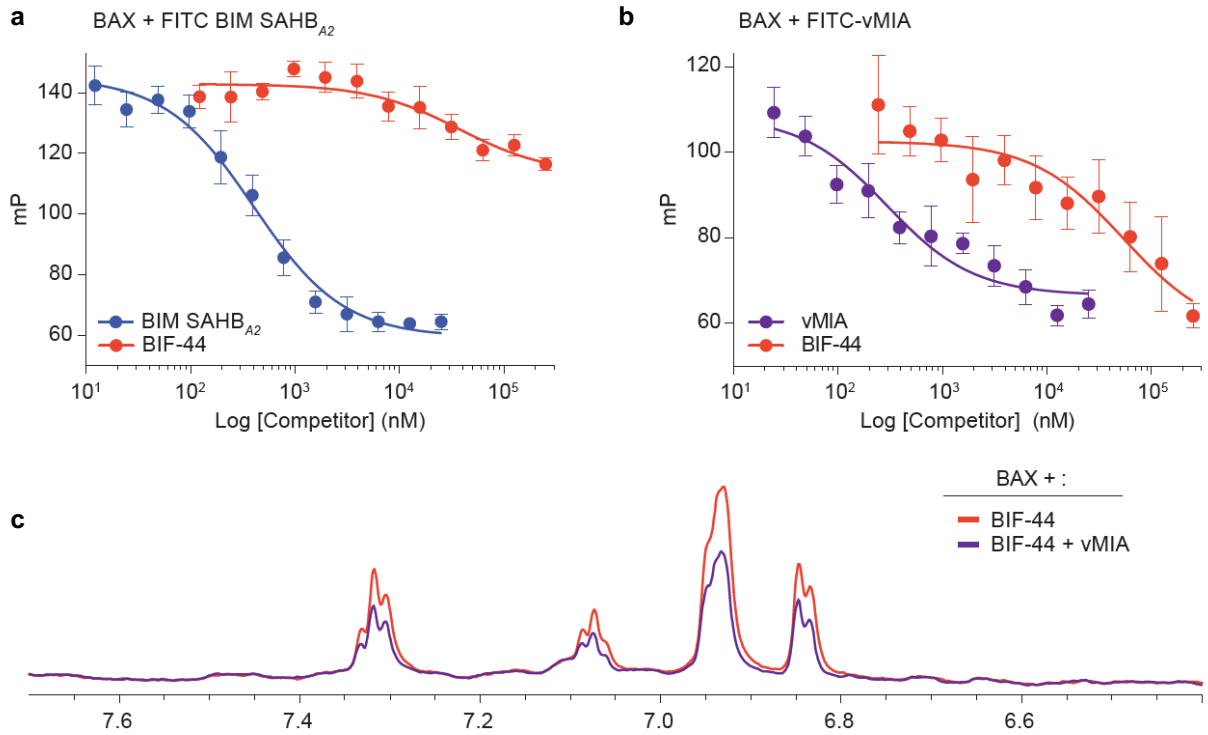

Figure 4-4: Competitive binding assays using BAX-binding peptides. (a,b) Competitive fluorescence polarization assays (FPA) demonstrate that BIF-44 does not effectively compete with FITC-BIM SAHBA2 for BAX interaction (a), but does compete with FITC-vMIA in dose-responsive fashion (b). The corresponding N-terminal acetylated peptides serve as positive controls for competition in each assay: Ac-BIM SAHBA2, blue (a); Ac-vMIA, purple (b). Error bars are mean ± SD for experiments performed in quadruplicate. (c) Competitive STD-NMR demonstrates suppression of the BIF-44 STD signal (red) upon co-incubation with vMIA peptide (purple), consistent with the competitive FPA results (a,b). FPA data from J. Pritz. Figure adapted from Pritz *et al.* (accepted).

4.3.4. Identification of the BIF-44 binding site on BAX

The BIF-44 binding site on BAX was more precisely defined using ^{15}N-BAX HSQC shift experiments. Upon titration with BIF-44, there are a series of focal, dose-responsive chemical shift changes that colocalize to the vMIA binding site on BAX (Figure 4-5). The most prominent changes (2 SD) localized to the junction of the α3-α4 and α5-α6 hairpins, which juxtapose to form a binding interface. Especially intriguing are more subtle changes (1 SD) that become amplified with increasing BIF-44 dosage and localize both to the internal helical regions of α5 and α6 (BAX's hydrophobic core), and the neighboring internal interaction surfaces between α1 and α2. This latter helix is the critical BH3 motif that must become

everted and exposed for BAX activation and oligomerization to ensue (40). To further develop a mechanistic hypothesis for the sensitization activity of BIF-44, the HSQC NMR results were used to guide a calculation of a docked structure of the BIF-44/BAX complex. These calculations predict that BIF-44 engages a deep pocket formed by the core hydrophobic α5 and

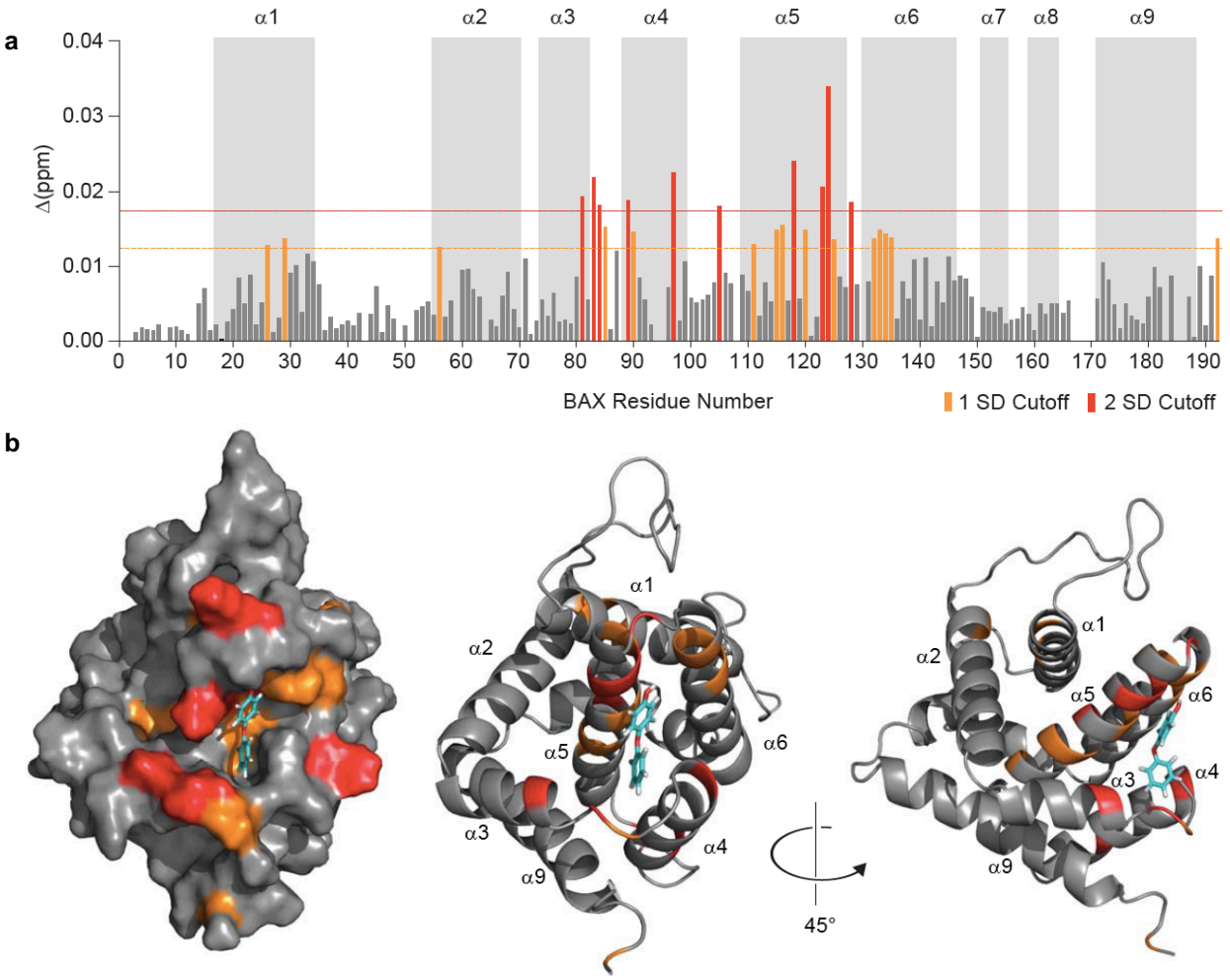

Figure 4-5: The BIF-44 Interaction Site on BAX Localizes to the vMIA-Binding Region. (a) Measured chemical shift changes of 15N- BAX upon addition of BIF-44 (6:1, BIF:BAX), plotted as a function of BAX residue number. The most prominent effects, reflecting chemical shift changes above the 2 SD cutoff (≥ 0.018 ppm significance threshold), are colored red and localize to the junction of the a3-a4 and a5-a6 hairpins. Significant changes at the 1 SD cutoff threshold (≥ 0.012 ppm significance threshold), are colored orange and encompass internal residues of the a5 and a6 core and discrete, juxtaposed residues of a1 and a2. (b) Residues that are represented as red and orange bars in the residue plot above are mapped accordingly onto the ribbon diagrams of monomeric BAX (PDB ID: 1F16). The most prominent chemical shift changes (2 SD cutoff) localize to the region implicated in the vMIA peptide (purple) interaction. A second cluster of chemical shift changes (1 SD cutoff) localize to internal and juxtaposed residues of a5, a6 and a1, a2, suggestive of allosteric sensing from the adjacent hydrophobic core to the a1-loop-a2 region of the BAX N-terminal face. BIF-44 is shown according to docking calculations based on the observed shifts. Figure adapted from Pritz *et al*. (accepted).

α6 helices and the loop between α3 and α4 (Figure 4-5B). Together, these results corroborate the STD and FP results localizing the interacting surface to the vMIA binding domain, and suggest that BIF-44 engagement induces structural reverberations transmitted through the α5-α6 hydrophobic core to the internal surfaces of α1 and α2.

4.3.5. BAX is sensitized by allosteric mobilization of the α1-α2 loop

The above results with BIF-44 present an intriguing question: how can a molecular fragment that sensitizes BH3-triggered BAX activation do so by engaging BAX in a region that mediates BAX inhibition? To explore this question, molecular dynamics simulations were conducted to assess protein movements in the presence or absence of BIF-44 at the docked site. These calculations suggest a specific increase in conformational flexibility involving the α1-α2 region of BAX (Figure 4-6), a site that is distant from the BIF-44 docking location but subject to allosteric sensing, as evidenced by the dose-responsive HSQC NMR results.

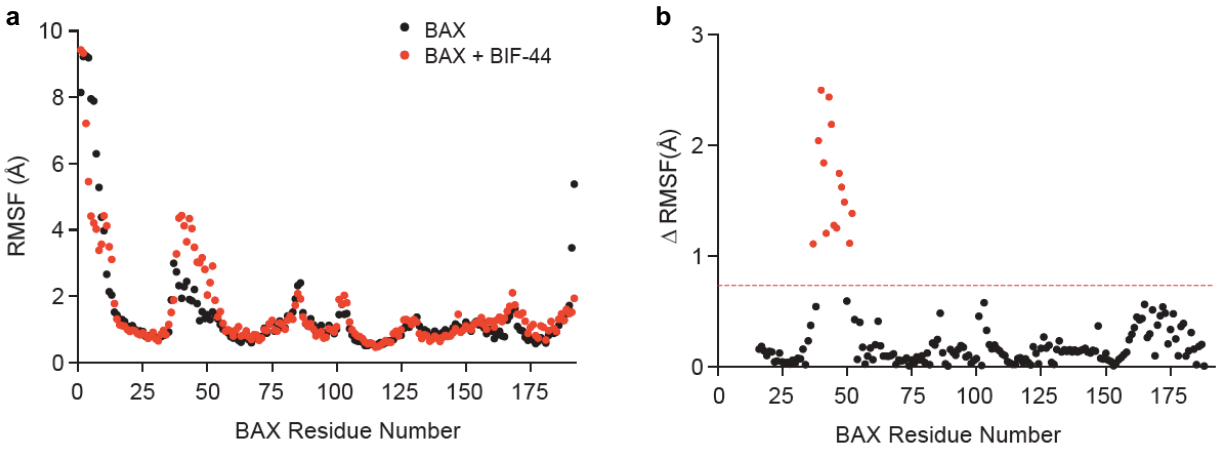

Figure 4-6: Molecular dynamics simulation showing the effect of BIF-44 binding on the conformational dynamics of BAX. (a) RMSF values for the Cα of each BAX residue over the course of the 100 ns molecular dynamics simulation for BAX in the presence (red) or absence (black) of BIF-44. (b) Absolute value of the difference in RMSF (ΔRMSF) between the unliganded and liganded forms of BAX. Residues above one SD threshold are shown in red, indicate increased mobility upon BIF-44 binding, and localize to the a1-a2 region of BAX. Residues from the unstructured portions at the N- and C-termini (residues 1-15 and 188-192, respectively) are excluded from the plot. Figure adapted from Pritz *et al*. (accepted).

4.4. Conclusions and future work

Allostery has emerged as a key feature of BCL-2 family protein regulation, influencing both the apoptotic response and opportunities to pharmacologically manipulate it. This work presents the first small molecule screen of full-length BAX in solution. Similar efforts were conducted over a decade ago decade ago for an anti-apoptotic BCL-2 family member, but an analogous approach applied to BAX has remained out of reach. The molecular fragment, BIF-44, identified by STD-NMR, has a unique BAX sensitization activity manifested upon co-incubation of the compound with BAX and a triggering BH3 ligand in a membrane environment. Paradoxically, the binding site for this molecule is not at one of the established BH3 interaction sites, but instead at a discrete region previously reported to mediate BAX inhibition by the cytomegalovirus vMIA protein. NMR analysis suggests that molecular engagement transmits chemical shift changes through the protein core to the N-terminal region of the protein that includes the BH3 helix. MD simulations further point to enhanced conformational flexibility of the α1-α2 region upon BIF-44 interaction.

These results suggest that molecular intercalation at the identified binding site, formed by the confluence of the α3-α4 and α5- α6 hairpins, represents a vulnerability for allosteric activation of BAX. Targeting and perturbing the α5/α6 hydrophobic core of the BAX protein in this manner provides both an opportunity to develop novel sensitizers of BAX-mediated apoptosis and a physiologic rationale for direct blockade of this site by BAX-inhibitory proteins such as vMIA. In addition, the allosteric consequences of BIF-44 sensitization, namely synergistic mobilization of the α1-α2 loop and BH3 domain, underscores the mechanistic importance of the N-terminal conformational change to BH3 initiation of BAX activation.

The identified fragment has very weak binding affinity, and is not expected to be selective for BAX or to have functional effect in cells. Nonetheless, it provides a starting point for additional medicinal chemistry efforts to develop a molecule with improved affinity and selectivity. This could include efforts to modify the existing fragment to develop a more ligand-like small molecule, or alternatively screening using other modalities to target the BIF-44 site. If such a molecule could be developed, it could be an important step in reactivating apoptosis in a range of human malignancies that are characterized by decreased cell death, making it an exciting potential therapeutic angle.

5. Overall conclusions and future directions

This thesis aimed to expand the range of apoptotic proteins targetable with small molecules. Significant efforts in this area have been conducted by labs and companies around the world since the discovery of human apoptotic targets, and fortunately for patients these efforts have been rewarded with the first FDA-approved BCL-2 inhibitor, venetoclax. Nonetheless, the vast majority of the intricate web of apoptotic proteins remains undrugged. The work in this thesis approached this problem from diverse, and atypical, directions in an attempt to complement existing efforts in the area. Stapled peptides are one key technology that enabled this work by providing high-affinity peptide ligands for the proteins of interest. Stapling allowed the native SOS1 peptide to be modified in Chapter 2 for greater affinity while retaining the existing binding site, and a high-affinity MCL-1 stapled peptide permitted the high-throughput screen that identified MAIM1 in Chapter 3. The development of improved stapled peptides remains a key focus in the Walensky lab, and molecules of this type are now in human clinical trials by Aileron Therapeutics. At this time there are no generalizable rules about the optimal position and properties of the staple, but future research will hopefully better elucidate the mechanism of stapled peptide entry into cells and how properties including helicity, hydrophobicity, and charge influence binding.

The work in Chapters 3 and 4 resulted from high-throughput screening efforts. MAIM1 was identified from a library containing more than 70,000 ligand-like members. The compound itself is a highly reactive, perhaps to the point that it is an undesirable member of a screening library that will be applied to numerous targets and may sit on a shelf to potentially degrade before the screen even begins. In this case, the molecule was useful not specifically as a ligand itself, but rather as a means of discovering a new allosteric site on the opposite face of MCL-1.

This required chemical intuition as to the reactivity of the molecule, combined with classical biochemical assays and MS analysis to confirm a covalent binding mechanism. While this work is only the first step towards confirming the utility of modifying MCL-1 at C286, it opens up a new angle for screening and rational design efforts that may complement existing drug discovery efforts.

Finally, Chapter 4 conducted the first reported fragment-based screen against full-length BAX. This effort required the growth of a large amount (>20 mg) of pure, monomeric BAX for screening with a library of c.a. 1000 small molecules. Due to difficulties with protein preparation, the screening of a larger library would be very difficult, so fragments allowed for the screening of a relatively large amount of chemical space within the constraints imposed by the protein. This screen resulted in the identification of a fragment, BIF-44 that sensitizes BAX to activation despite binding to an ordinarily inhibitory vMIA site. The identified molecule is small (MW c.a. 200 Da), and there is thus significant room for medicinal chemistry efforts to grow the fragment while remaining within drug-like space. It appears to act *via* an allosteric mechanism by exposing the distant $\alpha1$-$\alpha2$ loop, once again opening up a potential new site for small molecule therapeutics.

Taken together, this work presents the first efforts towards small molecules that modulate the activity of critical apoptotic proteins. It demonstrates how a combination of screening, computational design, biochemistry, and biophysical techniques can lead to a deeper understanding of these challenging targets.

6. Works cited

1. Blanpain C, Horsley V, Fuchs E. Epithelial stem cells: turning over new leaves. Cell. 2007 Feb 9;128(3):445–58.

2. Reed JC. Dysregulation of apoptosis in cancer. J Clin Oncol Off J Am Soc Clin Oncol. 1999 Sep;17(9):2941–53.

3. Hanahan D, Weinberg RA. The Hallmarks of Cancer. Cell. 2000 Jan 7;100(1):57–70.

4. Hanahan D, Weinberg RA. Hallmarks of Cancer: The Next Generation. Cell. 2011 Mar;144(5):646–74.

5. Kerr JFR, Wyllie AH, Currie AR. Apoptosis: A Basic Biological Phenomenon with Wide-ranging Implications in Tissue Kinetics. Br J Cancer. 1972 Aug;26(4):239–57.

6. Savill J, Fadok V. Corpse clearance defines the meaning of cell death. Nature. 2000 Oct 12;407(6805):784–8.

7. Sulston JE, Horvitz HR. Post-embryonic cell lineages of the nematode, Caenorhabditis elegans. Dev Biol. 1977 Mar;56(1):110–56.

8. Sulston JE, Schierenberg E, White JG, Thomson JN. The embryonic cell lineage of the nematode Caenorhabditis elegans. Dev Biol. 1983 Nov;100(1):64–119.

9. Ellis HM, Horvitz HR. Genetic control of programmed cell death in the nematode C. elegans. Cell. 1986 Mar 28;44(6):817–29.

10. Yuan J, Shaham S, Ledoux S, Ellis HM, Horvitz HR. The C. elegans cell death gene ced-3 encodes a protein similar to mammalian interleukin-1β-converting enzyme. Cell. 1993 Nov 19;75(4):641–52.

11. Hengartner MO, Ellis R, Horvitz R. Caenorhabditis elegans gene ced-9 protects cells from programmed cell death. Nature. 1992 Apr 9;356(6369):494–9.

12. Conradt B, Horvitz HR. The C. elegans Protein EGL-1 Is Required for Programmed Cell Death and Interacts with the Bcl-2–like Protein CED-9. Cell. 1998 May 15;93(4):519–29.

13. Liu X, Kim CN, Yang J, Jemmerson R, Wang X. Induction of Apoptotic Program in Cell-Free Extracts: Requirement for dATP and Cytochrome c. Cell. 1996 Jul 12;86(1):147–57.

14. Tsujimoto Y, Finger LR, Yunis J, Nowell PC, Croce CM. Cloning of the chromosome breakpoint of neoplastic B cells with the t(14;18) chromosome translocation. Science. 1984 Nov 30;226(4678):1097–9.

15. Tsujimoto Y, Cossman J, Jaffe E, Croce CM. Involvement of the bcl-2 gene in human follicular lymphoma. Science. 1985 Jun 21;228(4706):1440–3.

16. Hinds MG, Smits C, Fredericks-Short R, Risk JM, Bailey M, Huang DCS, et al. Bim, Bad and Bmf: intrinsically unstructured BH3-only proteins that undergo a localized conformational change upon binding to prosurvival Bcl-2 targets. Cell Death Differ. 2007 Jan;14(1):128–36.

17. Moldoveanu T, Grace CR, Llambi F, Nourse A, Fitzgerald P, Gehring K, et al. BID-induced structural changes in BAK promote apoptosis. Nat Struct Mol Biol. 2013 May;20(5):589–97.

18. Cheng EH-YA, Wei MC, Weiler S, Flavell RA, Mak TW, Lindsten T, et al. BCL-2, BCL-XL Sequester BH3 Domain-Only Molecules Preventing BAX- and BAK-Mediated Mitochondrial Apoptosis. Mol Cell. 2001 Sep;8(3):705–11.

19. Letai A, Bassik MC, Walensky LD, Sorcinelli MD, Weiler S, Korsmeyer SJ. Distinct BH3 domains either sensitize or activate mitochondrial apoptosis, serving as prototype cancer therapeutics. Cancer Cell. 2002 Sep;2(3):183–92.

20. Deng J, Carlson N, Takeyama K, Dal Cin P, Shipp M, Letai A. BH3 Profiling Identifies Three Distinct Classes of Apoptotic Blocks to Predict Response to ABT-737 and Conventional Chemotherapeutic Agents. Cancer Cell. 2007 Aug 14;12(2):171–85.

21. Moldoveanu T, Follis AV, Kriwacki RW, Green DR. Many players in BCL-2 family affairs. Trends Biochem Sci. 2014 Mar;39(3):101–11.

22. Souers AJ, Leverson JD, Boghaert ER, Ackler SL, Catron ND, Chen J, et al. ABT-199, a potent and selective BCL-2 inhibitor, achieves antitumor activity while sparing platelets. Nat Med. 2013 Feb;19(2):202–8.

23. Hannun YA. Apoptosis and the Dilemma of Cancer Chemotherapy. Blood. 1997 Mar 15;89(6):1845–53.

24. Roberts AW, Davids MS, Pagel JM, Kahl BS, Puvvada SD, Gerecitano JF, et al. Targeting BCL2 with Venetoclax in Relapsed Chronic Lymphocytic Leukemia. N Engl J Med. 2016 Jan 28;374(4):311–22.

25. van Delft MF, Wei AH, Mason KD, Vandenberg CJ, Chen L, Czabotar PE, et al. The BH3 mimetic ABT-737 targets selective Bcl-2 proteins and efficiently induces apoptosis via Bak/Bax if Mcl-1 is neutralized. Cancer Cell. 2006 Nov;10(5):389–99.

26. Beroukhim R, Mermel CH, Porter D, Wei G, Raychaudhuri S, Donovan J, et al. The landscape of somatic copy-number alteration across human cancers. Nature. 2010 Feb 18;463(7283):899–905.

27. Kozopas KM, Yang T, Buchan HL, Zhou P, Craig RW. MCL1, a gene expressed in programmed myeloid cell differentiation, has sequence similarity to BCL2. Proc Natl Acad Sci U S A. 1993 Apr 15;90(8):3516–20.

28. Krajewski S, Bodrug S, Krajewska M, Shabaik A, Gascoyne R, Berean K, et al. Immunohistochemical analysis of Mcl-1 protein in human tissues. Differential regulation of Mcl-1 and Bcl-2 protein production suggests a unique role for Mcl-1 in control of programmed cell death in vivo. Am J Pathol. 1995 Jun;146(6):1309–19.

29. Yang-Yen H-F. Mcl-1: a highly regulated cell death and survival controller. J Biomed Sci. 2006 Mar;13(2):201–4.

30. Willis SN, Chen L, Dewson G, Wei A, Naik E, Fletcher JI, et al. Proapoptotic Bak is sequestered by Mcl-1 and Bcl-xL, but not Bcl-2, until displaced by BH3-only proteins. Genes Dev. 2005 Jun 1;19(11):1294–305.

31. Certo M, Moore VDG, Nishino M, Wei G, Korsmeyer S, Armstrong SA, et al. Mitochondria primed by death signals determine cellular addiction to antiapoptotic BCL-2 family members. Cancer Cell. 2006 May;9(5):351–65.

32. Fire E, Gulla SV, Grant RA, Keating AE. Mcl-1-Bim complexes accommodate surprising point mutations via minor structural changes. Protein Sci Publ Protein Soc. 2010 Mar;19(3):507–19.

33. Liu G, Poppe L, Aoki K, Yamane H, Lewis J, Szyperski T. High-Quality NMR Structure of Human Anti-Apoptotic Protein Domain Mcl-1(171-327) for Cancer Drug Design. PLoS ONE. 2014 May 2;9(5):e96521.

34. Oltval ZN, Milliman CL, Korsmeyer SJ. Bcl-2 heterodimerizes in vivo with a conserved homolog, Bax, that accelerates programed cell death. Cell. 1993 Aug 27;74(4):609–19.

35. Sedlak TW, Oltvai ZN, Yang E, Wang K, Boise LH, Thompson CB, et al. Multiple Bcl-2 family members demonstrate selective dimerizations with Bax. Proc Natl Acad Sci. 1995 Aug 15;92(17):7834–8.

36. Hsu Y-T, Wolter KG, Youle RJ. Cytosol-to-membrane redistribution of Bax and Bcl-XL during apoptosis. Proc Natl Acad Sci. 1997 Apr 15;94(8):3668–72.

37. Edlich F, Banerjee S, Suzuki M, Cleland MM, Arnoult D, Wang C, et al. Bcl-xL Retrotranslocates Bax from the Mitochondria into the Cytosol. Cell. 2011 Apr 1;145(1):104–16.

38. Suzuki M, Youle RJ, Tjandra N. Structure of Bax: coregulation of dimer formation and intracellular localization. Cell. 2000 Nov 10;103(4):645–54.

39. Gavathiotis E, Suzuki M, Davis ML, Pitter K, Bird GH, Katz SG, et al. BAX activation is initiated at a novel interaction site. Nature. 2008 Oct 23;455(7216):1076–81.

40. Gavathiotis E, Reyna DE, Davis ML, Bird GH, Walensky LD. BH3-Triggered Structural Reorganization Drives the Activation of Proapoptotic BAX. Mol Cell. 2010 Nov 12;40(3):481–92.

41. Arnoult D, Bartle LM, Skaletskaya A, Poncet D, Zamzami N, Park PU, et al. Cytomegalovirus cell death suppressor vMIA blocks Bax- but not Bak-mediated apoptosis by binding and sequestering Bax at mitochondria. Proc Natl Acad Sci U S A. 2004 May 25;101(21):7988–93.

42. Ma J, Edlich F, Bermejo GA, Norris KL, Youle RJ, Tjandra N. Structural mechanism of Bax inhibition by cytomegalovirus protein vMIA. Proc Natl Acad Sci. 2012 Dec 18;109(51):20901–6.

43. Barclay LA, Wales TE, Garner TP, Wachter F, Lee S, Guerra RM, et al. Inhibition of Pro-apoptotic BAX by a noncanonical interaction mechanism. Mol Cell. 2015 Mar 5;57(5):873–86.

44. Saraogi I, Hamilton AD. α-Helix mimetics as inhibitors of protein–protein interactions. Biochem Soc Trans. 2008 Dec;36(6):1414.

45. Ross NT, Katt WP, Hamilton AD. Synthetic mimetics of protein secondary structure domains. Philos Trans R Soc Math Phys Eng Sci. 2010 Mar 13;368(1914):989–1008.

46. Cunningham B, Wells J. High-resolution epitope mapping of hGH-receptor interactions by alanine-scanning mutagenesis. Science. 1989 Jun 2;244(4908):1081–5.

47. Wells JA, McClendon CL. Reaching for high-hanging fruit in drug discovery at protein-protein interfaces. Nature. 2007 Dec 13;450(7172):1001–9.

48. Villoutreix BO, Labbé CM, Lagorce D, Laconde G, Sperandio O. A leap into the chemical space of protein-protein interaction inhibitors. Curr Pharm Des. 2012;18(30):4648–67.

49. Cohen NA, Stewart ML, Gavathiotis E, Tepper JL, Bruekner SR, Koss B, et al. A Competitive Stapled Peptide Screen Identifies a Selective Small Molecule that Overcomes MCL-1-Dependent Leukemia Cell Survival. Chem Biol. 2012 Sep 21;19(9):1175–86.

50. Friberg A, Vigil D, Zhao B, Daniels RN, Burke JP, Garcia-Barrantes PM, et al. Discovery of potent myeloid cell leukemia 1 (Mcl 1) inhibitors using fragment based methods and structure based design. J Med Chem. 2013 Jan 10;56(1):15–30.

51. Joseph TL, Lane DP, Verma CS. Stapled BH3 Peptides against MCL-1: Mechanism and Design Using Atomistic Simulations. PLoS ONE. 2012 Aug 31;7(8):e43985.

52. Muppidi A, Doi K, Edwardraja S, Drake EJ, Gulick AM, Wang H-G, et al. Rational Design of Proteolytically Stable, Cell-Permeable Peptide-Based Selective Mcl-1 Inhibitors. J Am Chem Soc. 2012 Sep 12;134(36):14734–7.

53. Varadarajan S, Vogler M, Butterworth M, Dinsdale D, Walensky LD, Cohen GM. Evaluation and critical assessment of putative MCL-1 inhibitors. Cell Death Differ. 2013 Nov;20(11):1475–84.

54. Stanfield RL, Wilson IA. Protein-peptide interactions. Curr Opin Struct Biol. 1995 Feb;5(1):103–13.

55. Koh JT, Cornish VW, Schultz PG. An Experimental Approach to Evaluating the Role of Backbone Interactions in Proteins Using Unnatural Amino Acid Mutagenesis. Biochemistry (Mosc). 1997 Sep 1;36(38):11314–22.

56. Kutzki O, Park HS, Ernst JT, Orner BP, Yin H, Hamilton AD. Development of a Potent Bcl-xL Antagonist Based on α-Helix Mimicry. J Am Chem Soc. 2002 Oct 1;124(40):11838–9.

57. Yin H, Lee G-I, Sedey KA, Kutzki O, Park HS, Orner BP, et al. Terphenyl-Based Bak BH3 alpha-helical proteomimetics as low-molecular-weight antagonists of Bcl-xL. J Am Chem Soc. 2005 Jul 27;127(29):10191–6.

58. Ernst JT, Becerril J, Park HS, Yin H, Hamilton AD. Design and Application of an α-Helix-Mimetic Scaffold Based on an Oligoamide-Foldamer Strategy: Antagonism of the Bak BH3/Bcl-xL Complex. Angew Chem Int Ed. 2003;42(5):535–539.

59. Yin H, Hamilton AD. Terephthalamide derivatives as mimetics of the helical region of Bak peptide target Bcl-xL protein. Bioorg Med Chem Lett. 2004 Mar 22;14(6):1375–9.

60. Rodriguez JM, Hamilton AD. Benzoylurea Oligomers: Synthetic Foldamers That Mimic Extended α Helices. Angew Chem Int Ed. 2007 Nov;46(45):8614–7.

61. Rodriguez JM, Nevola L, Ross NT, Lee G, Hamilton AD. Synthetic Inhibitors of Extended Helix–Protein Interactions Based on a Biphenyl 4,4′-Dicarboxamide Scaffold. ChemBioChem. 2009;10(5):829–833.

62. Biros SM, Moisan L, Mann E, Carella A, Zhai D, Reed JC, et al. Heterocyclic α-helix mimetics for targeting protein–protein interactions. Bioorg Med Chem Lett. 2007 Aug 15;17(16):4641–5.

63. Walensky LD, Kung AL, Escher I, Malia TJ, Barbuto S, Wright RD, et al. Activation of Apoptosis in Vivo by a Hydrocarbon-Stapled BH3 Helix. Science. 2004 Sep 3;305(5689):1466–70.

64. Bird GH, Madani N, Perry AF, Princiotto AM, Supko JG, He X, et al. Hydrocarbon double-stapling remedies the proteolytic instability of a lengthy peptide therapeutic. Proc Natl Acad Sci. 2010 Aug 10;107(32):14093–8.

65. Stewart ML, Fire E, Keating AE, Walensky LD. The MCL-1 BH3 helix is an exclusive MCL-1 inhibitor and apoptosis sensitizer. Nat Chem Biol. 2010 Aug;6(8):595–601.

66. Walensky LD, Bird GH. Hydrocarbon-Stapled Peptides: Principles, Practice, and Progress. J Med Chem. 2014 Aug 14;57(15):6275–88.

67. Okamoto T, Zobel K, Fedorova A, Quan C, Yang H, Fairbrother WJ, et al. Stabilizing the Pro-Apoptotic BimBH3 Helix (BimSAHB) Does Not Necessarily Enhance Affinity or Biological Activity. ACS Chem Biol. 2013 Feb 15;8(2):297–302.

68. Bird GH, Gavathiotis E, Labelle JL, Katz SG, Walensky LD. Distinct BimBH3 (BimSAHB) Stapled Peptides for Structural and Cellular Studies. ACS Chem Biol. 2014 Jan 3;

69. Okamoto T, Segal D, Zobel K, Fedorova A, Yang H, Fairbrother WJ, et al. Further Insights into the Effects of Pre-organizing the BimBH3 Helix. ACS Chem Biol [Internet]. 2014 Feb 18 [cited 2014 Feb 25]; Available from: http://dx.doi.org/10.1021/cb400638p

70. Edwards AL, Wachter F, Lammert M, Huhn AJ, Luccarelli J, Bird GH, et al. Cellular Uptake and Ultrastructural Localization Underlie the Pro-apoptotic Activity of a Hydrocarbon-stapled BIM BH3 Peptide. ACS Chem Biol. 2015 Sep 18;10(9):2149–57.

71. Singh J, Petter RC, Baillie TA, Whitty A. The resurgence of covalent drugs. Nat Rev Drug Discov. 2011 Apr;10(4):307–17.

72. Chalker JM, Bernardes GJL, Lin YA, Davis BG. Chemical Modification of Proteins at Cysteine: Opportunities in Chemistry and Biology. Chem – Asian J. 2009 May 4;4(5):630–40.

73. Marino SM, Gladyshev VN. Cysteine function governs its conservation and degeneration and restricts its utilization on protein surface. J Mol Biol. 2010 Dec 17;404(5):902–16.

74. Rucker AL, Pager CT, Campbell MN, Qualls JE, Creamer TP. Host-guest scale of left-handed polyproline II helix formation. Proteins Struct Funct Bioinforma. 2003;53(1):68–75.

75. Guharoy M, Chakrabarti P. Secondary structure based analysis and classification of biological interfaces: identification of binding motifs in protein-protein interactions. Bioinforma Oxf Engl. 2007 Aug 1;23(15):1909–18.

76. Pauling L, Corey RB, Branson HR. The Structure of Proteins. Proc Natl Acad Sci U S A. 1951 Apr;37(4):205–11.

77. Dunitz JD. Pauling's Left-Handed α-Helix. Angew Chem Int Ed. 2001 Nov 19;40(22):4167–73.

78. Kendrew JC, Dickerson RE, Strandberg BE, Hart RG, Davies DR, Phillips DC, et al. Structure of Myoglobin: A Three-Dimensional Fourier Synthesis at 2 |[angst]|. Resolution. Nature. 1960 Feb 13;185(4711):422–7.

79. Schafmeister CE, Po J, Verdine GL. An All-Hydrocarbon Cross-Linking System for Enhancing the Helicity and Metabolic Stability of Peptides. J Am Chem Soc. 2000 Jun 1;122(24):5891–2.

80. Walensky LD, Pitter K, Morash J, Oh KJ, Barbuto S, Fisher J, et al. A Stapled BID BH3 Helix Directly Binds and Activates BAX. Mol Cell. 2006 Oct 20;24(2):199–210.

81. Leshchiner ES, Parkhitko A, Bird GH, Luccarelli J, Bellairs JA, Escudero S, et al. Direct inhibition of oncogenic KRAS by hydrocarbon-stapled SOS1 helices. Proc Natl Acad Sci. 2015 Feb 10;112(6):1761–6.

82. Bernal F, Tyler AF, Korsmeyer SJ, Walensky LD, Verdine GL. Reactivation of the p53 Tumor Suppressor Pathway by a Stapled p53 Peptide. J Am Chem Soc. 2007 Mar 1;129(9):2456–7.

83. Vo U, Embrey KJ, Breeze AL, Golovanov AP. 1H, 13C and 15N resonance assignment for the human K-Ras at physiological pH. Biomol NMR Assign. 2012 Aug 12;7(2):215–9.

84. Williamson MP. Using chemical shift perturbation to characterise ligand binding. Prog Nucl Magn Reson Spectrosc. 2013 Aug;73:1–16.

85. de Vries SJ, van Dijk M, Bonvin AMJJ. The HADDOCK web server for data-driven biomolecular docking. Nat Protoc. 2010 May;5(5):883–97.

86. Wassenaar TA, Dijk M van, Loureiro-Ferreira N, Schot G van der, Vries SJ de, Schmitz C, et al. WeNMR: Structural Biology on the Grid. J Grid Comput. 2012 Nov 30;10(4):743–67.

87. Margarit SM, Sondermann H, Hall BE, Nagar B, Hoelz A, Pirruccello M, et al. Structural Evidence for Feedback Activation by Ras·GTP of the Ras-Specific Nucleotide Exchange Factor SOS. Cell. 2003 Mar 7;112(5):685–95.

88. Rossi AM, Taylor CW. Analysis of protein-ligand interactions by fluorescence polarization. Nat Protoc. 2011 Mar;6(3):365–87.

89. Karnoub AE, Weinberg RA. Ras oncogenes: split personalities. Nat Rev Mol Cell Biol. 2008 Jul;9(7):517–31.

90. Stephen AG, Esposito D, Bagni RK, McCormick F. Dragging Ras Back in the Ring. Cancer Cell. 2014 Mar 17;25(3):272–81.

91. Chardin P, Camonis JH, Gale NW, Aelst L van, Schlessinger J, Wigler MH, et al. Human Sos1: a guanine nucleotide exchange factor for Ras that binds to GRB2. Science. 1993 May 28;260(5112):1338–43.

92. van Zundert GCP, Rodrigues JPGLM, Trellet M, Schmitz C, Kastritis PL, Karaca E, et al. The HADDOCK2.2 Web Server: User-Friendly Integrative Modeling of Biomolecular Complexes. J Mol Biol. 2016 Feb 22;428(4):720–5.

93. Bird GH, Mazzola E, Opoku-Nsiah K, Lammert MA, Godes M, Neuberg DS, et al. Biophysical determinants for cellular uptake of hydrocarbon-stapled peptide helices. Nat Chem Biol. 2016 Oct;12(10):845–52.

94. Lee S, Wales TE, Escudero S, Cohen DT, Luccarelli J, Gallagher CG, et al. Allosteric inhibition of antiapoptotic MCL-1. Nat Struct Mol Biol. 2016 Jun;23(6):600–7.

95. Ge Y, Kazi A, Marsilio F, Luo Y, Jain S, Brooks W, et al. Discovery and Synthesis of Hydronaphthoquinones as Novel Proteasome Inhibitors. J Med Chem. 2012 Mar 8;55(5):1978–98.

96. Sastry GM, Adzhigirey M, Day T, Annabhimoju R, Sherman W. Protein and ligand preparation: parameters, protocols, and influence on virtual screening enrichments. J Comput Aided Mol Des. 2013 Mar 1;27(3):221–34.

97. Shelley JC, Cholleti A, Frye LL, Greenwood JR, Timlin MR, Uchimaya M. Epik: a software program for pK a prediction and protonation state generation for drug-like molecules. J Comput Aided Mol Des. 2007 Dec 1;21(12):681–91.

98. Jorgensen WL, Chandrasekhar J, Madura JD, Impey RW, Klein ML. Comparison of simple potential functions for simulating liquid water. J Chem Phys. 1983 Jul 15;79(2):926–35.

99. Jorgensen WL, Maxwell DS, Tirado-Rives J. Development and Testing of the OPLS All-Atom Force Field on Conformational Energetics and Properties of Organic Liquids. J Am Chem Soc. 1996 Jan 1;118(45):11225–36.

100. Essmann U, Perera L, Berkowitz ML, Darden T, Lee H, Pedersen LG. A smooth particle mesh Ewald method. J Chem Phys. 1995 Nov 15;103(19):8577–93.

101. Hoover WG. Canonical dynamics: Equilibrium phase-space distributions. Phys Rev A. 1985 Mar 1;31(3):1695–7.

102. Martyna GJ, Tobias DJ, Klein ML. Constant pressure molecular dynamics algorithms. J Chem Phys. 1994 Sep 1;101(5):4177–89.

103. Humphreys DD, Friesner RA, Berne BJ. A Multiple-Time-Step Molecular Dynamics Algorithm for Macromolecules. J Phys Chem. 1994 Jul 1;98(27):6885–92.

104. Guo Z, Mohanty U, Noehre J, Sawyer TK, Sherman W, Krilov G. Probing theα-Helical Structural Stability of Stapled p53 Peptides: Molecular Dynamics Simulations and Analysis. Chem Biol Drug Des. 2010 Apr;75(4):348–59.

105. Baell J, Walters MA. Chemistry: Chemical con artists foil drug discovery. Nat News. 2014 Sep 25;513(7519):481.

106. Engen JR. Analysis of Protein Conformation and Dynamics by Hydrogen/Deuterium Exchange MS. Anal Chem. 2009 Oct 1;81(19):7870–5.

107. Verdine GL, Walensky LD. The Challenge of Drugging Undruggable Targets in Cancer: Lessons Learned from Targeting BCL-2 Family Members. Clin Cancer Res. 2007 Dec 15;13(24):7264–70.

108. Lee EF, Czabotar PE, Yang H, Sleebs BE, Lessene G, Colman PM, et al. Conformational Changes in Bcl-2 Pro-survival Proteins Determine Their Capacity to Bind Ligands. J Biol Chem. 2009 Oct 30;284(44):30508–17.

109. Leshchiner ES, Braun CR, Bird GH, Walensky LD. Direct activation of full-length proapoptotic BAK. Proc Natl Acad Sci. 2013 Mar 12;110(11):E986–95.

110. Zhu K, Borrelli KW, Greenwood JR, Day T, Abel R, Farid RS, et al. Docking covalent inhibitors: a parameter free approach to pose prediction and scoring. J Chem Inf Model. 2014 Jul 28;54(7):1932–40.

111. Ostrem JM, Peters U, Sos ML, Wells JA, Shokat KM. K-Ras(G12C) inhibitors allosterically control GTP affinity and effector interactions. Nature. 2013 Nov 28;503(7477):548–51.

112. Hajduk PJ, Greer J. A decade of fragment-based drug design: strategic advances and lessons learned. Nat Rev Drug Discov. 2007 Mar;6(3):211–9.

113. Gavathiotis E, Reyna DE, Bellairs JA, Leshchiner ES, Walensky LD. Direct and selective small-molecule activation of proapoptotic BAX. Nat Chem Biol. 2012 Jul;8(7):639–45.

114. Harder E, Damm W, Maple J, Wu C, Reboul M, Xiang JY, et al. OPLS3: A Force Field Providing Broad Coverage of Drug-like Small Molecules and Proteins. J Chem Theory Comput. 2016 Jan 12;12(1):281–96.

115. Friesner RA, Murphy RB, Repasky MP, Frye LL, Greenwood JR, Halgren TA, et al. Extra Precision Glide: Docking and Scoring Incorporating a Model of Hydrophobic Enclosure for Protein−Ligand Complexes. J Med Chem. 2006 Oct 1;49(21):6177–96.

116. Mayer M, Meyer B. Characterization of Ligand Binding by Saturation Transfer Difference NMR Spectroscopy. Angew Chem Int Ed. 1999 Jun 14;38(12):1784–8.